International Journal of Pharmaceutics 624 (2022) 122030

Contents lists available at ScienceDirect

International Journal of Pharmaceutics

journal homepage: www.elsevier.com/locate/ijpharm

Impact of solvent dry down, vehicle pH and slowly reversible keratin binding on skin penetration of cosmetic relevant compounds: I. Liquids

Kevin Tonnis [a], Johannes M. Nitsche [b], Lijing Xu [c], Alison Haley [a], Joanna Jaworska [d], Gerald B. Kasting [c,*]

[a] College of Engineering and Applied Science, The University of Cincinnati, Cincinnati, OH 45221, USA
[b] Department of Chemical and Biological Engineering, University at Buffalo, The State University of New York, Buffalo, NY 14260–4200, USA
[c] The James L. Winkle College of Pharmacy, The University of Cincinnati, Cincinnati, OH 45267-0514, USA
[d] The Procter & Gamble Company, Data and Modeling Sciences, Brussels Innovation Center, Belgium

ARTICLE INFO

Keywords:
Absorption
Biophysical models
Dermal delivery
Disposition
Percutaneous
Transdermal
Skin

ABSTRACT

To measure progress and evaluate performance of the newest UB/UC/P&G skin penetration model we simulated an 18-compound subset of finite dose in vitro human skin permeation data taken from a solvent-deposition study of cosmetic-relevant compounds (Hewitt et al., J. Appl. Toxicol. 2019, 1–13). The recent model extension involved slowly reversible binding of solutes to stratum corneum keratins. The selected subset was compounds that are liquid at skin temperature. This set was chosen to distinguish between slow binding and slow dissolution effects that impact solid phase compounds. To adequately simulate the physical experiments there was a need to adjust the evaporation mass transfer coefficient to better represent the diffusion cell system employed in the study. After this adjustment the model successfully predicted both dermal delivery and skin surface distribution of 12 of the 18 compounds. Exceptions involved compounds that were cysteine-reactive, highly water-soluble or highly ionized in the dose solution. Slow binding to keratin, as presently parameterized, was shown to significantly modify the stratum corneum kinetics and diffusion lag times, but not the ultimate disposition, of the more lipophilic compounds in the dataset. Recommendations for further improvement of both modeling methods and experimental design are offered.

1. Introduction

Compounds employed in cosmetic and personal care products must be safe for topical application on humans, yet they often contain reactive functional groups that introduce an element of intrinsic hazard. Prominent examples are fragrances, preservatives and hair dye components or their precursors. The industry places enormous effort into risk assessment for these compounds through corporate research and also through industry-supported organizations including Cosmetics Europe (CE), the Research Institute for Fragrance Materials (RIFM) and the Personal Care Products Council (PCPC). Based on the paradigm that Risk = Hazard × Exposure, significant effort is put into the evaluation of both external and internal exposure. Dermal absorption provides the link between these two metrics. Williams and coworkers present a recent example of how flux through the skin can be used to determine systemic risk relative to oral absorption (Williams et al., 2016). Other efforts include building a measure of epidermal bioavailability into multi-assay strategies for assessing skin sensitization hazard and risk (Basketter et al., 2007; Jaworska et al., 2015).

Given this environment, it is not surprising that considerable effort has been placed on developing predictive models for dermal absorption including the estimation of transient tissue levels in the stratum

Abbreviations: ADME, absorption, distribution, metabolism and excretion; BE, 2-butoxyethanol; CBA, 4-chlorobutyric acid; CDC, Center for Disease Control; CE, Cosmetics Europe; DD, dermal delivery; DE, dermis; DEA, diethanolamine; DEGBE, diethyleneglycol monobutyl ether; DPRA, direct peptide reactivity assay; ED, viable epidermis; EHA, 2-ethylhexylacetate; GHS, global harmonized system; kDPRA, kinetic direct peptide reactivity assay; MMS, methyl methanesulfonate; mp, melting point; MVA, 4-methylvaleric acid; PBS, phosphate-buffered saline; PCPC, Personal Care Products Council; PPRA, peroxidase/peroxide-activated peptide reactivity assay; P_{vp}, vapor pressure; RF, receptor fluid; RIFM, Research Institute for Fragrance Materials; SC, stratum corneum; SI, Supplementary Information; TGA, thioglycolic acid; UB/UC, University at Buffalo/University of Cincinnati.

* Corresponding author at: The James L. Winkle College of Pharmacy, University of Cincinnati Academic Health Center, Cincinnati, OH 45247-0514, USA.
E-mail addresses: kastingb@ucmail.uc.edu, Gerald.Kasting@uc.edu (G.B. Kasting).

https://doi.org/10.1016/j.ijpharm.2022.122030
Received 6 May 2022; Received in revised form 29 June 2022; Accepted 14 July 2022
Available online 18 July 2022

corneum (SC), viable epidermis (ED) and dermis (DE). These models, which are strongly grounded in experiment, offer the possibility of predicting absorption in cases involving as-yet-untested chemical agents and formulations, dermal loading and exposure times. A variety of accessible models (at least 10) are available at the time of this writing.

This report provides an update on the model developed within our group, which was first published in its entirety in 2013 (Dancik et al., 2013), but contains components dating to a decade earlier. We will refer to the Dancik et al. model as UB/UC, for the institutions involved in its development. With the help of industry partner Procter & Gamble, UB/UC was migrated to the gPROMS® process engineering platform in 2014, where its capabilities have been significantly extended. These include the ability to model transient skin hydration through a continuous uptake and loss of water (Li et al., 2016; Li et al., 2015; Saadatmand et al., 2017), the ability to quantitatively handle highly polar solutes (Kasting et al., 2019; Yu et al., 2021; Yu et al., 2022), and the ability to simultaneously model the disposition of two diffusing components, including solutes that precipitate on the skin surface during dry down (Yu et al., 2022). We will refer to the extended model as UB/UC/P&G and herein introduce a versioning system to clarify the updates.

In the present report we have extended the UB/UC/P&G model to include the impact of slowly reversible binding of diffusing solutes to SC proteins, particularly keratin. We hypothesize that this phenomenon plays a role in the long-recognized skin property commonly termed "stratum corneum reservoir" (Vickers, 1963, 1972). This subject has been treated quantitatively by several research groups (Anissimov and Roberts, 2009; Frasch et al., 2011; Nitsche and Frasch, 2011; Seif and Hansen, 2012), and was recently revisited by ours (Nitsche and Kasting, 2022). This report implements the most recent analysis and examines its impact on the transient skin absorption of chemicals relevant to cosmetic and personal care products.

The test dataset was selected from compounds included in the recent in vitro finite dose skin penetration study published by Hewitt et al. (Hewitt et al., 2019). This study comprises one leg of a three-part study of 56 cosmetic relevant compounds commissioned by the Cosmetics Europe ADME Task Force. The other two legs provide physical properties measurements (Grégoire et al., 2017) and steady state partition coefficients and skin permeability coefficients (Ellison et al., 2020). We will refer to this dataset collectively as the "CE dataset". In order to clearly distinguish slowly reversible keratin binding from the additional delay associated with slow dissolution of precipitated solids on the skin surface – also a feature of the CE dataset (Hamadeh et al., 2021) – we chose to confine the present analysis to solutes that are liquids when in their neat state at a skin temperature of 32°.

2. Mathematical model

The skin disposition model employed in this study builds on a one-dimensional model developed by our group on the gPROMS® platform to predict the transient absorption and evaporation rates of a binary solute/solvent combination applied to the skin (Yu et al., 2021; Yu et al., 2022). The model comprises a vehicle layer, three skin layers and a follicular pathway in parallel with the composite skin pathway. The steady state properties of the model have been thoroughly explored in Models 1 (Kasting et al., 2019) and 2 (Yu et al., 2021). The most recent version of this model, Model 3 (Yu et al., 2022), has herein been revised to include slowly reversible keratin binding for the solute, replacing the assumption of rapidly equilibrated binding in Models 1–3. We also include a careful treatment of ionizable compounds to represent the ionization equilibrium throughout a transient process during which the vehicle gradually evaporates. Features included in Models 1–3 have been retained. We will refer to the present model as Model 4. Notably, Model 4 is a two-state model describing skin in either partially hydrated or fully hydrated states. The skin swelling feature described in (Li et al., 2015) is not implemented. Furthermore, the dissolution limitation on solvent-deposited solids described in (Yu et al., 2022) is not invoked, as the analysis involves only liquid solutes. In order to bring clarity to the continuing evolution of this code we have introduced a versioning system that is described in Table S1 of the Supplementary Information (SI).

2.1. Slowly reversible binding in the stratum corneum

In Models 1–3, keratin binding of both the solute and the solvent in the SC was assumed to instantly reach equilibrium, whereas Model 4 accounts for the binding kinetics of the solute according to a newly developed analysis (Nitsche and Kasting, 2022). Nitsche and Kasting considered three length scales related to keratin binding – ultrascopic, microscopic and macroscopic – thereby enabling more accurate conversion of "on" and "off" binding rate constants measured on isolated keratins to diffusion kinetics in the SC (cf. Fig. 1). The ultrascopic scale involves processes occurring at the interface between keratin microfibrils and water, microscopic refers to phase-specific properties relating to lipid and protein regions of the SC, and macroscopic refers to tissue-averaged properties (SC only) that are accessible by common IVPT procedures. We employ below the nomenclature introduced in (Nitsche and Kasting, 2022) in which properties pertaining to the ultrascopic scale have no overbar, those pertaining to the microscopic scale have one overbar, and those pertaining to the macroscopic scale have two overbars. This nomenclature is applied here only to the SC layer of the skin, although in principle one could also extend it to the lower skin layers since the effective diffusivities and partition coefficients therein also include free and bound fractions (Kretsos et al., 2008). We furthermore limit the ultrascopic description to the corneocyte phase only, as the corresponding ultrascopic model of the lipid phase is embedded within the microscopic model previously described (Nitsche et al., 2006; Wang et al., 2007). We are not aware of experimental evidence to suggest that organic compounds bind in a noncovalent manner to SC lipids, although it has been shown that small amounts of water bind tightly to SC lipid headgroups – see (Yadav et al., 2007) and references therein. Consequently, we limit the description of binding to SC proteins, cognizant of the fact that this phenomenon may include cornified cell envelope proteins as well as keratin.

In Model 4 both the solvent and solute are considered to have slow binding characteristics described by the equations that follow. This choice allows for an eventual transition to more complex vehicles in

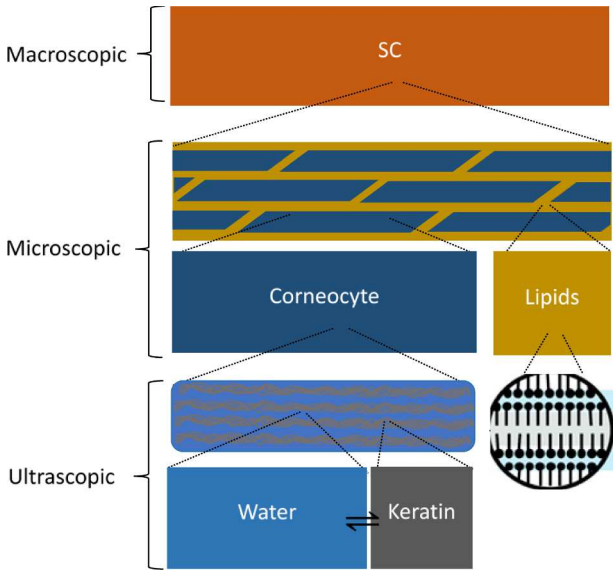

Fig. 1. Schematic diagram of the three levels of homogenization (ultrascopic, microscopic and macroscopic) represented in the Model 4 skin diffusion model. Transport and partitioning variables applying to the stratum corneum layer at each level of detail are represented in the text with 0, 1 or 2 overbars, respectively.

which the binary solution limitation is removed. Anissimov and Roberts have proposed slow binding kinetics for water in the SC, supported by ^3H_2O transport experiments conducted at constant skin hydration (Anissimov and Roberts, 2009). We believe incorporation of their model directly in the absence of a true skin swelling model, e.g. (Li et al., 2015), to describe the transient swelling during the dry down process would be premature. The equations below are furthermore written to include the case of ionizable solutes, which are not discussed in (Nitsche and Kasting, 2022), but were explicitly considered by Hansen and coworkers (Hansen et al., 2011; Seif and Hansen, 2012). As in Hansen's work, only nonionized solutes are considered to bind to keratin. We write equations for the solute only to simplify the description.

The evolution of solute concentration in the SC is governed by the equations (Nitsche and Kasting, 2022)

$$\frac{\partial \overline{\overline{C}}^{sc}}{\partial t} = \frac{\overline{\overline{D}}^{sc}\partial^2\overline{\overline{C}}^{sc}}{\partial z^2} - \overline{\overline{k}}_{on}^{sc}\overline{\overline{C}}^{sc} + \overline{\overline{k}}_{off}^{sc}\overline{\overline{B}}^{sc} + j^{inf,sc} \tag{1}$$

$$\partial\overline{\overline{B}}^{sc} \Big/ \partial t = \overline{\overline{k}}_{on}^{sc}\overline{\overline{C}}^{sc} - \overline{\overline{k}}_{off}^{sc}\overline{\overline{B}}^{sc} \tag{2}$$

where $\overline{\overline{C}}^{sc}(z,t)$ is the superficial concentration of free (mobile, diffusible, unbound) solute in the SC, $\overline{\overline{B}}^{sc}(z,t)$ is the superficial concentration of solute bound to keratin, $\overline{\overline{k}}_{on}^{sc}$ and $\overline{\overline{k}}_{off}^{sc}$ are the forward ("on") and reverse ("off") rate constants for binding and unbinding, respectively, and $j^{inf,sc}$ is the flux from the infundibulum into the SC. The qualifier 'superficial' means amount of solute per total tissue volume, not broken down into microscopic lipid and proteinaceous compartments, which are not discernable at the macroscopic scale. The $j^{inf,sc}$ term is associated with a hair follicle transport pathway that is not considered in (Nitsche and Kasting, 2022), but may be found in (Yu et al., 2021).

The macroscopic diffusion coefficient, $\overline{\overline{D}}^{sc}$, is calculated from the equation.

$$\overline{\overline{D}}^{sc} = \left(P^{sc/w}\right)^{comp} h^{sc} \Big/ \overline{\overline{K}}_{free}^{sc/w} \tag{3}$$

where $\left(P^{sc/w}\right)^{comp}$ denotes the macroscopically observable steady state permeability coefficient of the SC, h^{sc} the thickness of the SC, and $\overline{\overline{K}}_{free}^{sc/w}$ the effective SC/water partition coefficient of freely diffusing solute. The value of $\overline{\overline{K}}_{free}^{sc/w}$ is calculated as

$$\overline{\overline{K}}_{free}^{sc/w} = \overline{\phi}^{lip}\overline{K}^{lip/w} + \overline{\phi}^{cor}\overline{K}_{free}^{cor/w} \tag{4}$$

in which $\overline{\phi}^{lip}$ and $\overline{\phi}^{cor}$ are the volume fractions occupied by the microscopic lipid and corneocyte phases, and $\overline{K}^{lip/w}$, $\overline{K}_{free}^{cor/w}$ are the partition coefficients of freely diffusing solute in these phases relative to an aqueous reference solution. The partition coefficients follow directly from (Nitsche et al., 2006) after accounting for ionization as in (Kasting et al., 2019) (see their Eq. (21)):

$$\overline{K}^{lip/w} = 0.43\left(K^{o/w}\right)^{0.81} \tag{5}$$

$$\overline{K}_{free}^{cor/w} = \left[\frac{\upsilon}{\left(\omega^{ker}\rho^{w}/\rho^{ker}\right) + \upsilon}\right] \Big/ \left(f_{non}^{cor}\right)_{free}$$

for an infinitesimally small solute

$$= \left(1 - \phi^{ker}\right) \Big/ \left(f_{non}^{cor}\right)_{free} \qquad \text{for an infinitesimally small solute} \tag{6}$$

Here $\left(f_{non}^{cor}\right)_{free}$ is the nonionized fraction of freely diffusing solute in the aqueous phase of the corneocyte at the SC pH (default 5.5) and ϕ^{ker} is the volume fraction of keratin fibers in a corneocyte. The nonionized fraction $\left(f_{non}^{cor}\right)_{free}$ is easily calculated, as it is equivalent to f_{non} in an aqueous solution, e.g. $f_{non} = \left(1 + 10^{\mathrm{pH}-\mathrm{p}K_a}\right)^{-1}$ for a weak acid. Equations (3) and (4) differ from the corresponding relationships in (Nitsche et al., 2006) in that $\overline{\overline{D}}^{sc}$ and $\overline{\overline{K}}_{free}^{sc/w}$ refer specifically to freely diffusing solute, whereas the earlier parameters applied to free + bound solute. Equation (6) is analogous to Eq. (C1) in (Nitsche et al., 2006), which was written therein as applying only to water as a solute. The superscript "pro" in Eq. (C1) has been changed to "ker" for consistency with the present nomenclature. Refinement of Eq. (6) for finite-sized solutes is described in the Appendix.

All discussion so far refers to the average macroscopic properties of the SC, distinguished by the superscript "sc" and having two overbars. A key question important for practical applications is how to link these properties to the fundamental ultrascopic properties of keratin-water dispersions, henceforth distinguished by the superscript "ker" and having no overbars. Such dispersions make up the interiors of corneocytes, contributing to the SC reservoir, and are amenable to experiments characterizing binding to isolated keratin substrates.

Seif and Hansen (Seif and Hansen, 2012) developed a relationship giving k_{off}^{ker} as a function of the equilibrium binding constant, K_{eq}^{ker}, for bovine horn and hoof keratin (cf. their Eq. (10)),

$$\frac{1}{k_{off}^{ker}\left[\mathrm{min}^{-1}\right]} = 25.75\ \mathrm{min} + (0.459\ \mathrm{min})K_{eq}^{ker} \tag{7}$$

The units in Eq. (7) are inferred from Seif and Hansen's Fig. 4a. The equilibrium binding constant K_{eq}^{ker} is the ratio of the ultrascopic binding to unbinding rate constants, $k_{on}^{ker}/k_{off}^{ker}$. It is equivalent to the ion-corrected protein/water partition coefficient, $PC^{pro/\mathrm{pH}}$, which can be estimated by adjusting Nitsche et al.'s correlation for $PC^{pro/w}$ (Eq. (11) in (Nitsche et al., 2006)) for ionization, i.e.

$$K_{eq}^{ker} \equiv PC^{pro/\mathrm{pH}} = \left(f_{non}^{cor}\right)_{free}\left[5.4\left(K^{o/w}\right)^{0.27}\right] \tag{8}$$

Because the unbinding rate constant does not vary with scale (Nitsche and Kasting, 2022) (their Eq. (41)), the macroscopically observable unbinding constant, $\overline{\overline{k}}_{off}^{sc}$, can be calculated directly from Eq. (7), i.e. $\overline{\overline{k}}_{off}^{sc} = k_{off}^{ker}$. The value of the ultrascopic binding rate constant k_{on}^{ker} can then calculated as the product of k_{off}^{ker} and K_{eq}^{ker}. This value is then converted to the macroscopic binding rate constant, $\overline{\overline{k}}_{on}^{sc}$ using Nitsche and Kasting's Eq. (40) (Nitsche and Kasting, 2022), i.e.

$$\overline{\overline{k}}_{on}^{sc} = k_{on}^{ker}\cdot\left(\frac{\overline{\phi}^{cor}\overline{K}_{free}^{cor/w}}{\overline{\phi}^{cor}\overline{K}_{free}^{cor/w} + \overline{\phi}^{lip}\overline{K}^{lip/w}}\cdot\frac{\rho^{ker}}{\rho^{w}}\cdot\frac{\phi^{ker}}{1-\phi^{ker}}\right) \tag{9}$$

for an infinitesimally small solute

where ρ^{ker} is the density of keratin, ρ^{w} is the density of water, and ϕ^{ker} is the volume fraction of the corneocyte occupied by keratin. Inserting Eq. (6) into Eq. (9), we find after rearrangement

$$\overline{\overline{k}}_{on}^{sc} = k_{on}^{ker}\cdot\left(\frac{\left(\rho^{ker}/\rho^{w}\right)\phi^{ker}}{\left(f_{non}^{cor}\right)_{free}\left(\overline{\phi}^{lip}/\overline{\phi}^{cor}\right)\overline{K}^{lip/w} + \left(1-\phi^{ker}\right)}\right) \qquad \text{for an infinitesimally small solute.} \tag{10}$$

Similarly to Eq. (6), Eq. (10) also incurs an adjustment for finite-sized solutes, as described in the Appendix.

The difference between the propagation of the ultrascopic rate constants, k_{off}^{ker} and k_{on}^{ker}, to macroscopic constants, $\overline{\overline{k}}_{off}^{sc}$ and $\overline{\overline{k}}_{on}^{sc}$, is not obvious. It can be explained as follows (Nitsche and Kasting, 2022): "…the concentration basis used for bound solute (per keratin mass, or per total keratin dispersion or tissue volume) does not affect the "off" (unbinding) rate constant. This outcome is consistent with the notion that the mean survival time of a bound solute molecule as an entity stuck to the surface of a keratin microfibril, and therefore the first-order kinetics of its detachment, would appear to be an attribute of the adsorption process independent of the volumetric distribution and number density of microfibrils. However, the "on" (binding) rate constant is strongly influenced by the concentration basis used…".

The initial conditions within the SC are given by

$$\overline{\overline{C}}^{sc}(z,0) = \begin{cases} \overline{\overline{C}}_0^{sc} & 0 \le z \le fh^{sc} \\ 0 & fh^{sc} < z \le h^{sc} \end{cases} \tag{11}$$

$$\overline{\overline{B}}^{sc}(z,0) = 0 \qquad 0 \le z \le h^{sc} \tag{12}$$

Here f is the fraction of the SC considered to be the deposition layer, the part of the SC that is sufficiently permeable that dose solution immediately penetrates following application (Hamadeh et al., 2021; Kasting and Miller, 2006), and

$$\overline{\overline{C}}_0^{sc} = \left(C_0^v / K^{v/w}\right) \cdot \overline{\overline{K}}_{free}^{sc/w} \tag{13}$$

is the free solute concentration in the SC that is at equilibrium with the initial concentration of the dose solution, C_0^v. The partition coefficient $K^{v/w}$ corrects for nonaqueous vehicles or aqueous vehicles leading to an ionization state other than the nonionized solute in water. For an aqueous solution in which the solute is partially ionized, $K^{v/w} = \left(f_{non}^v\right)^{-1}$ (Kasting et al., 2019).

The boundary conditions at the base of the SC are given by the equations.

$$\overline{\overline{D}}^{sc} \cdot \frac{\partial \overline{\overline{C}}^{sc}(h^{sc},t)}{\partial z} = D^{ed} \cdot \frac{\partial C^{ed}(h^{sc},t)}{\partial z} \tag{14}$$

$$\overline{\overline{C}}^{sc}(h^{sc},t) \Big/ \overline{\overline{K}}_{free}^{sc/w} = C^{ed}(h^{sc},t) \Big/ K_{free}^{ed/w} \tag{15}$$

The boundary conditions at the surface of the SC vary according to the state of dry down, as described in the next section. Values of the constant parameters used in Eqs. (1)–(15) are given in Table 1.

Table 1
Parameter values associated with stratum corneum (SC) layer of the diffusion model.

Property	Description	Fully Hydrated	Partially Hydrated	Ref
h^{sc}	Stratum corneum thickness, μm	43.4	13.4	a
υ	Mass of water/mass of dry SC	2.75	0.43	b
$\overline{\phi}^{lip}$	Lipid fraction of the SC	0.0316	0.0927	b
$\overline{\phi}^{cor}$	Corneocyte fraction of the SC	0.9684	0.9073	b
ϕ^{ker}	Keratin fraction of the corneocyte	0.1928	0.6044	b, c
ρ^w	Density of water, g/cm^3	1.0		b, c
ρ^{ker}	Density of keratin, g/cm^3	1.37		b, c

[a] (Wang et al., 2006); (Wang et al., 2007).
[b] (Nitsche et al., 2006).
[c] (Nitsche and Kasting, 2022).

2.2. Partitioning and dry down of formulation at the skin surface

The representation of formulation kinetics in Model 4 builds on that described in (Miller and Kasting, 2015), later modified by (Yu et al., 2022) (Model 3). Miller and Kasting described a multicomponent vehicle with all components miscible but one – the solute of interest. Yu et al. limited the composition to two components, but added a follicular pathway, dissolution-limited kinetics for solid precipitates, and the capability to handle ionized or partially ionized solutes. In these models, as well as Model 4, the solvent persists at the start of the simulation and dissipates by evaporation and penetration based on its vapor pressure and activity in the presence of dissolved solute. As a result, the boundary conditions at the skin surface vary depending on the saturation state of the vehicle, and whether either the solute or solvent has completely dissipated. A small fraction of the formulation flows into the upper part of the hair follicle (the infundibulum) and deposits its contents there (Yu et al., 2022). Fig. 2 shows a schematic of the possible surface states that can develop during the course of a topical application.

Here, we describe the early stages of the dissipation process and how they vary from those in the previously cited references and – importantly – from those in (Hamadeh et al., 2021), who also used a two-component vehicle model in their recent analysis of the full CE dataset. For liquids, the slow binding model offers a complementary interpretation to Hamadeh et al.'s finding that the solute deposition layer has lower capacity than that predicted from (Dancik et al., 2013). For clarity we discuss only the equilibrium between a well-stirred vehicle containing a nonionized solute and solvent at the SC/vehicle interface. Elaborations regarding the follicular infundibulum are described in (Yu et al., 2022) and more detail on multicomponent vehicle thermodynamics may be found in Appendix 1 of (Miller and Kasting, 2015). Adjustments for ionization are discussed in Section 2.3 and evaporation is discussed in Section 2.5.

When the binary formulation contacts the skin in Model 4, there is immediate partitioning of both the solvent (Species 1) and the solute (Species 2) into the SC deposition layer, taken, as in (Dancik et al., 2013), to be the upper 10 % of the SC for partially hydrated skin and the upper 2.5 % for fully hydrated skin. However, the partitioning of both species is governed by Eqs. (4), (11) and (13) rather than by thermodynamic equilibria as described by (Miller and Kasting, 2015). In other words, partition equilibrium involves only the freely diffusing components, $\overline{\overline{C}}_1^{sc}$ and $\overline{\overline{C}}_2^{sc}$, as expressed by Eq. (13). Binding to yield species $\overline{\overline{B}}_1^{sc}$ and $\overline{\overline{B}}_2^{sc}$ begins immediately after deposition at a rate governed by Eqs. (2) and (7)–(10) with the exception of water, for which $K_{eq,1}^{ker} \equiv PC^{pro/pH} = 0$, yielding $\overline{\overline{B}}_1^{sc} = 0$. To avoid an unrealistically high sorption of water-miscible organic solvents and other highly water-soluble solutes, $\overline{\overline{K}}_{eq,1}^{sc/w}$ is limited to ρ /3, where $\overline{\overline{K}}_{eq,1}^{sc/w}$ is the equilibrium SC/water partition coefficient (including both free and bound species) and ρ is the density of the neat chemical. This value supported experimentally for the ethanol/water system, cf. Fig. 2 in (Berner et al., 1989) and serves as a practical limitation for other chemicals.

These limitations deserve a comment. The argument why $K_{eq,1}^{ker}$ (or $PC^{pro/w}$) should be zero for water was presented in Appendix C of (Nitsche et al., 2006), cf. their Eq. (C1) or the present Eq. (6). Water is a special case, as it is also the solvent that hydrates keratin. Slowly reversible binding of water can be observed (Anissimov and Roberts, 2009), but it does not impact the total amount of water in the SC. Rather, it simply partitions the total amount of water into free and bound subsets (Nitsche et al., 2006). Somewhat different arguments apply to the limitation on $\overline{\overline{K}}_{eq,1}^{sc/w}$ for water-miscible solvents (e.g. ethanol and acetone) and other highly water-soluble solutes. Chief among these is the fact that direct application of Eq. (8) leads to enormous predicted absorption of these solvents when the external concentration is high and binding equilibrium has been achieved. Although some co-swelling occurs with

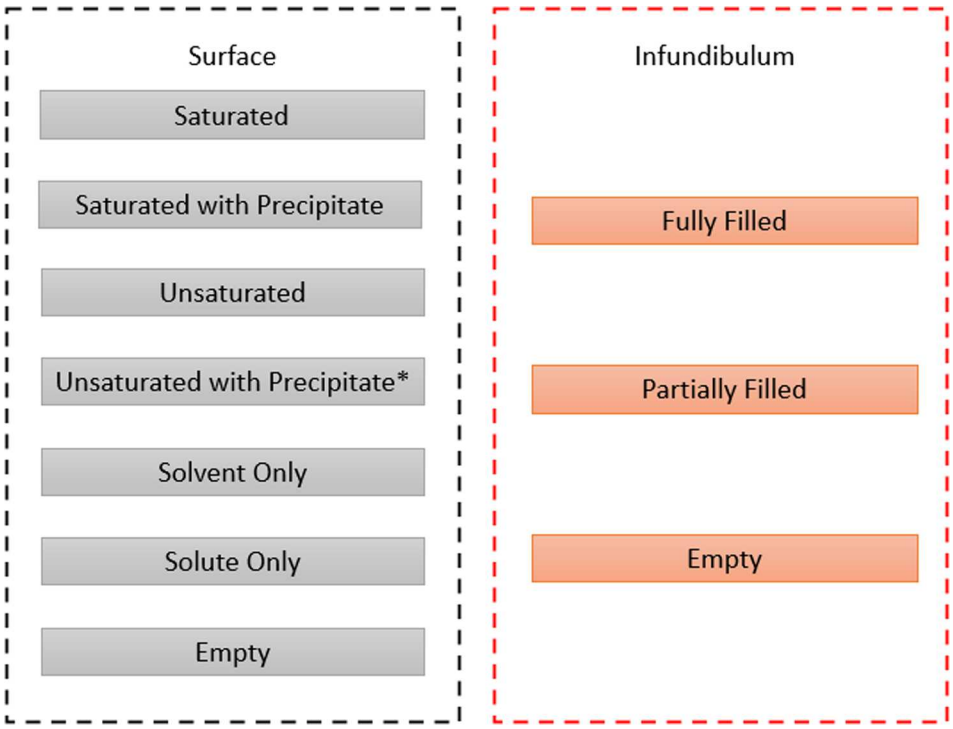

Fig. 2. Diagram representing the possible states of the topically-applied formulation during the dry down process. Asterisk identifies a case not currently possible, but which would occur were additional components in the vehicle to be considered.

ethanol (Berner et al., 1989), it is modest compared to that predicted by the blind use of Eq. (8). Large amounts of neat ethanol actually de-swell the SC (Berner et al., 1989), whereas extended exposure to ethanol, acetone or other more aggressive solvents disrupts or extracts SC lipids and increases skin permeability (Scheuplein, 1978). Further arguments are presented in Section 7.3. More precise treatment of transient absorption of these chemicals awaits the development of true multicomponent skin swelling models comparable to that for water (Li et al., 2015).

2.3. Treatment of ionized compounds

Models 1–4 allows for the transport of both neutral and ionized species through the skin. Transport rates are very sensitive to ionization, so the ionization equilibria must be carefully traced at the skin surface and at each layer of the skin. The fraction nonionized of each permeant is calculated separately for each skin layer and the vehicle based on the local pH of that layer. Default pH values in Models 1–4 are 5.5 for SC and 7.4 for ED and DE. The vehicle is considered to have a constant pH equal to the initial pH of the dose solution while the solvent is present. For nonaqueous solvents it is assumed that no ionization is possible above the skin surface.

The pH of the SC warrants a comment. It is well established that the natural pH of the SC surface in vivo falls in the range 5.0–5.5, based on measurement with surface electrodes. This is known as the skin's "acid mantle" and is an important component of the skin's antimicrobial barrier as well as regulation of desquamatory enzymes (Fluhr and Elias, 2002). Furthermore, a low pH environment is maintained throughout the SC based on fluorescence measurements with pH-sensitive dyes (Hanson et al., 2002). But topically-applied formulations having a different pH can alter the SC pH for a period of several hours, depending on the dose. This is the basis for several different measurements of skin buffer capacity (Levin and Maibach, 2008; Miller and Kasting, 2022). In the present analysis, satisfactory predictions of weak electrolyte permeation were obtained by maintaining an SC pH of 5.5, combined with a "hard solids" approximation for deposited salts as described in Section 5.4.3; however, only few compounds were affected. We reserve the right to eventually modify this approximation in order to accommodate a broader dataset.

2.4. Highly water-soluble compounds

For highly water-soluble compounds that attain high concentrations in an aqueous vehicle, the dilute solution approximations embodied in Eqs. (3), (4), (13) and (15) (i.e. that partition coefficients are constant and independent of concentration) are no longer valid. Direct application of these relationships leads to concentrations within the SC much higher than physically possible. In Model 4 we avoid this problem by limiting the maximum concentration of the permeant in the SC to 1/3rd of its density as discussed in Section 2.2. This constraint is enforced by reducing the SC/vehicle partition coefficient at the beginning of the calculation, after which it is held constant. This approximation is analogous to that applied for niacinamide in (Yu et al., 2022), except it is empirically- rather than thermodynamically-based. The value of 1/3rd draws from Berner et al.'s study of the mutual partitioning of ethanol and water into human SC (Berner et al., 1989). Although this approximation underestimates the partition coefficient when the vehicle is very dilute, most of the penetration occurs when the vehicle becomes concentrated, so the partition coefficient for a saturated solution yields a reasonable solution to the problem.

It can be shown that a concentration-dependent partition coefficient necessarily leads to a concentration-dependent diffusion coefficient, yielding changes to the governing equation for mass transport even more complex than those for the spatially-dependent diffusion and partition coefficients described by Anissimov and Roberts (Anissimov and Roberts, 2004). While this is an interesting development to contemplate, implementation of such a model architecture without a strong understanding of the concentration dependence is not likely to be productive.

The concentration limitation ultimately lowers the value of $\overline{\overline{K}}_{free}^{sc/w}$ (Eq. (4)). One then must choose whether to allow the value of $\overline{\overline{D}}^{sc}$ to increase

at high concentrations, as predicted by Eq. (3), or to proportionately reduce $(P^{sc/w})^{comp}$ and maintain the dilute solution value of $\overline{\overline{D}}^{sc}$. For the organic solvents ethanol and acetone we allowed $\overline{\overline{D}}^{sc}$ to increase. For solutes not expected to perturb the barrier we maintained its dilute solution value. Water itself is a special case as discussed in Section 2.2 and Appendix C of (Wang et al., 2006).

2.5. Evaporation from skin surface

An additional feature implemented in Model 4 considers that ionized species do not evaporate. Therefore, evaporation rates of volatile solutes from the vehicle (when present) or skin surface are scaled by the fraction nonionized at that layer. Other than that, evaporative loss from the binary vehicle is calculated as in (Miller and Kasting, 2015), with some small adjustments for the area of follicular openings. Bearing in mind that surface conditions vary with the state of dry down as shown in Fig. 1, we choose as an example the case where an unsaturated solution containing both components resides on the skin surface and the infundibulum is fully filled. The evaporative flux j_{evap} from the vehicle is given by

$$j_{evap(i)} = k_{evap(i)}\rho_i\left(\frac{a_i}{a_i^{sat}}\right), \qquad i = 1,2 \qquad (1 = \text{solvent}, 2 = \text{solute}) \tag{16}$$

where ρ_i is the density of Component i and $a_i = \gamma_i X_i$ is its thermodynamic activity. For liquids, $a_i^{sat} = 1$, whereas for solids, $a_i^{sat} < 1$ (Miller and Kasting, 2015). The liquid phase evaporation mass transfer coefficients $k_{evap(i)}$ are given by (Yu et al., 2022).

$$k_{evap(i)} = k_{g(i)}\frac{P_{vp(i)}\mathrm{MW}_i}{\rho_i RT} \quad i = 1, 2 \tag{17}$$

where $k_{g(i)}$ is the gas phase mass transfer coefficient which depends on the wind velocity, u:

$$k_{g(i)} = \frac{0.01756u^{0.78}}{(\mathrm{MW}_i)^{1/3}} \quad i = 1, 2 \tag{18}$$

The default indoor (or benchtop) value for wind velocity in Models 3 and 4 is $u = 0.10$ m/s and outdoor (or fume hood) value is $u = 0.50$ m/s. These values are lower than those recommended by Gajjar et al. (Gajjar et al., 2013), for reasons discussed in Section 5.1.

When the surface of the skin no longer has either excess solute or solvent present, the boundary condition on the top of the skin is based on evaporative flux at $z = 0$,

$$j_{evap(i)}(0) = \frac{k_{evap(i)}\rho_i\overline{\overline{C}}_i^{sc}(0)f_{non(i)}^{sc}}{\overline{\overline{C}}_i^{sc,sat}} \quad i = 1, 2 \tag{19}$$

Here $\overline{\overline{C}}_i^{sc}(0)$ is the macroscopic average concentration (or "superficial concentration" – see Eqs. (1) and (2)) of free Component i at the surface of the skin, and $\overline{\overline{C}}_i^{sc,sat}$ is its saturation value in the SC. Since the vapor pressure of ionized solute is considered to be negligible, the operative concentration governing evaporation at the surface of the SC is approximated by $\overline{\overline{C}}_i^{sc}(0)f_{non(i)}^{sc}$.

3. Methods

3.1. Experimental dataset

The test compounds were selected from the 56-compound dataset described by (Hewitt et al., 2019) and are shown in Table 2. The criterion for selection was a melting point less than 32 °C. Physical properties in Table 2 are those from the Supplementary Table 1 in (Hewitt et al., 2019), supplemented by calculations of molar volume, V_A, density ρ and fraction unbound in a 2 % albumin solution, f_u. In some instances physical properties from other sources were substituted for those in (Hewitt et al., 2019) as noted in the table. The activity coefficients, γ, used to calculate the activity in equation (16) were estimated using COSMOtherm 2021. Because COSMOtherm's predictions for solubility do not match the measured values that were used in these simulations, the activity coefficients were scaled so that the activity of solute in a saturated solution will equal 1, which is an appropriate choice for liquid solutes. CAS numbers and SMILES for the selected compounds can be found in Table S6 in the SI.

Table 2
Physicochemical properties of solutes in CE liquids dataset (Hewitt et al., 2019).

Chemical	MW	V_A[a] cm³/mol	ρ[b] g/cm³	mp, °C	pK_a	Donor soln pH	Donor soln f_{non}	f_u[c]	S_w, mg/ml	log $K^{o/w}$	Volatility P_{vp}, mmHg	% recovery[d]
2-Ethylhexyl acrylate	184.3	245		−90	–	7	1	0.21	1.27	4.09	1.78E−01	56
4-Chlorobutyric acid	122.6	122.5	1.24	16	4.5 HA	6	0.031	0.22	82.19	1.32	4.88E−02	50
4-Methylvaleric acid	116.2	147		−33	4.8 HA	6.8	0.01	0.18	8.48	1.98	1.41E−01	20
4-Tolunitrile	117.2	140		28.1	–	7.1	1	0.77	0.79	2.09	3.13E−01	19
Acetophenone	120.2	140		19.6	–	7.6	1	0.30	8.86	1.58	3.97E−01	7
Anisyl alcohol	138.2	154		24.3	–	7	1	0.56	2	1.1	1.80E−03	89
Benzyl bromide	171	143.5		−3.1	–	6.6	1	0.36	7.32	2.92	4.50E−01	14
Diethanolamine	105.1	126		27.9	8.71 BH^+	7	0.019	0.95	1000	−1.43	2.82E−04	95
Diethyleneglycol monobutyl ether	162.2	203		−68	–	7.2	1	0.85	495	0.56	2.19E−02	2
Diethylmaleate	172.2	189		−6.8	–	7.2	1	0.20	15.45	2.2	1.05E−01	19
Dimethyl phthalate	194.2	196		4.4	–	7	1	0.58	3.18	1.6	3.08E−03	77
Eugenol	164.2	189		−9.7	10.3 HA	7	1	0.67	3.21	2.27	2.26E−02	71
Geraniol	152.2	217	0.89	−15	–	7	1	0.63	0.35	3.56	3.00E−02	22
Isoeugenol	164.2	189		11.8	10.1 HA	7	0.999	0.71	0.6	3.04	1.20E−02	81
Methyl methane sulfonate	110.1	112		20	–	7	1	0.76	530.5	−0.5	4.14E−01	11
Nitrobenzene	123.1	119		5.5	–	7	1	0.62	4.69	1.85	2.45E−01	11
Thioglycolic acid	92.1	84		−15.1	3.7 HA	6	0.005	0.42	471.6	0.09	8.68E−02	77
trans-Cinnamaldehyde	132.2	154		−7.6	–	ND	1	0.79	1.4	1.9	3.84E−02	43

[a] Molar volume at the normal boiling point by Schröder's method (Poling et al., 2001).
[b] Density at 32 °C.
[c] Calculation based on ACD Labs value of K_a^{HSA} assuming a 2 % (0.6 mM) albumin solution according to $f_u = \left[1 + \left(6 \times 10^{-4}\right)K_a^{HSA}\right]^{-1}$
[d] Volatility pre-test (Gregoire et al., 2019).

Table 3
Skin disposition and mass balance for Cosmetics Europe dataset (Hewitt et al., 2019).

Compound	Dose, μg/cm^2	Vehicle	Fume hood?	Skin Wash, %	SC, %	ED, %	DE, %	Total Receptor, %	Mass Balance, %	Calc Evap, %
2-Ethylhexyl acrylate	6.63	0.01 M PBS + AOs	Yes	25.23	1.02	0.29	0.09	3.04	29.66	70.34
4-Chlorobutyric acid	66.36	0.1 M PBS	Yes	82.64	3.92	5.71	0.74	5.52	98.53	1.47
4-Methylvaleric acid	20.3	0.1 M PBS	Yes	15.36	0.17	0.1	0.052	21.98	37.66	62.34
4-Tolunitrile	1.89	0.01 M PBS	Yes	2.26	0.04	0.03	0.01	17.25	19.6	80.4
Acetophenone	10.27	0.1 M PBS	Yes	1.95	0.11	0.06	0.00	13.81	15.90	84.10
Anisyl alcohol	11.95	0.01 M PBS	No	4.84	0.11	0.07	0.16	85.00	90.18	9.82
Benzyl bromide	9.12	100 % acetone	Yes	2.59	0.64	1.23	0.81	1.18	6.44	93.56
Diethanolamine	10.2	0.01 M PBS + AOs	No	96.85	1.31	1.22	0.14	0.57	99.81	0.19
Diethyleneglycol monobutyl ether	64.11	0.1 M PBS	Yes	1.03	0.13	0.05	0.00	11.98	13.19	86.81
Diethylmaleate	24.08	0.1 M PBS	Yes	12.97	1.08	0.73	0.2	26.78	41.75	58.25
Dimethyl phthalate	1.31	0.01 M PBS	Yes	16	0.93	0.27	0.06	61.69	78.95	21.05
Eugenol	6.23	0.1 M PBS + AOs	Yes	4.73	0.79	0.09	0.07	58.64	64.33	35.67
Geraniol (PBS)	2.36	0.01 M PBS	Yes	5.56	0.35	0.17	0.24	32.01	34.34	65.66
Geraniol (Ethanol)	2.92	100 % ethanol	Yes	26.28	0.54	0.09	0.08	3.97	30.96	69.04
Isoeugenol	3.52	0.1 M PBS + AOs	Yes	17.06	1.28	0.6	0.49	67.82	87.25	12.75
Methyl methane sulfonate	24.83	0.1 M PBS	Yes	8.69	1	0.47	0.09	3.9	14.15	85.85
Nitrobenzene	3.7	0.01 M PBS	Yes	7.5	1.71	0.49	0.22	23.19	33.13	66.87
Thioglycolic acid	72.46	0.1 M PBS	No	65.85	5.97	2.05	0.99	11.08	85.93	14.07
trans-Cinnamaldehyde	2.42	0.1 M PBS	No	3.99	0.9	0.91	0.36	55.14	61.3	38.7

[a] Evaporated percentage calculated as 100 % − Mass Balance.
[b] AOs = antioxidants (3 % ascorbic acid and 0.4 % sodium sulfite).

Dose information and the distribution of the compounds following a 24 h topical application to excised human surgical skin mounted in Franz diffusion cells are shown in Table 3. These data were extracted from the more extensive tables provided by (Hewitt et al., 2019) and (Gregoire et al., 2019). % evaporated is calculated as (100 – Mass balance) as in (Gregoire et al., 2019).

3.2. Model assumptions and parameters

The fully hydrated skin option (h_{sc} = 43.3 μm, $H_{trans} = H_{lat} = 1$) was selected for all calculations involving an aqueous dose solvent, and the partially hydrated skin option (h_{sc} = 13.4 μm, $H_{trans} = H_{lat} = 3$) was selected for calculations with an ethanol or acetone dose solvent. Here h_{sc} is SC thickness and H_{trans} and H_{lat} are divisors that adjust the transverse mass transfer coefficient and lateral diffusivity of diffusing species in SC lipids, decreasing their values for partially hydrated skin (Wang et al., 2007). The basis for this choice is explained in Section 4.1. As in Model 3, it was assumed that both solvent and solute were uniformly dispersed on the skin surface as a well-stirred solution or suspension until the final stage of dry down (vehicle thickness $h_v < 25$ μm), after which lateral transport in the vehicle was not allowed. This "surface roughness limitation" prevents unrealistically high accumulation of solute in the hair follicles (Yu et al., 2022). The receptor fluid (RF) was considered to be a perfect sink. Phosphate-buffered saline (PBS) dose solutions were modeled as binary solutions of solutes in water having a constant pH equal to the measured dose pH prior to the study. The pH in the SC, ED, and DE was assumed to remain constant throughout the experiment at values of 5.5, 7.4 and 7.4, respectively.

The default Model 3 and 4 values for wind velocity of $u = 0.10$ and 0.50 m/s were employed for benchtop and fume hood experiments, respectively. However, the related evaporative mass transfer coefficient, k_g (cf. Eqs. (17) and (18)), for all experiments was optimized for this analysis as described in the next section.

To evaluate the influence of follicular delivery on the results, simulations were conducted using the default Model 3 value of 24 hairs/cm^2 (Kasting et al., 2022) and then rerun in the absence of hair follicles. As in (Kasting et al., 2022) all of the follicles were considered to be "closed". This differs from our earlier steady-state analyses in which a small fraction (1.5 %) of the follicles were considered to be open at the base of the infundibulum in order to accommodate permeation of very large molecules (Kasting et al., 2019; Yu et al., 2021). The dermal delivery resulting from the two calculations was compared. Dermal delivery is defined in Section 4.3.

3.3. Optimization of evaporative mass transfer

Evaporative mass transfer is sensitive to the temperature, the ambient air flow (u), the geometry of the evaporating surface and the vapor pressure of the evaporating species as captured in Eqs. (16)–(18) and discussed in more detail elsewhere (Frasch et al., 2018; Frasch and Bunge, 2015; Gajjar et al., 2013). Preliminary analyses of the data in Table 3, combined with a study of previous analyses including these data using variants of the UB/UC model (Gregoire et al., 2021; Hamadeh et al., 2021), therein called Dancik et al. 2013 and CDC, indicated that the default Model 4, on average, underpredicted initial solute permeation rates and overpredicted evaporation rates. To calibrate Model 4 to the particular conditions of the CE experiments, a two-step procedure was employed.

Calibration proceeded as follows. A multiplier, α_{trans} or α_g, was inserted into the code preceding the variables k_{trans} and k_g, respectively. The lipid phase transverse mass transfer coefficient, k_{trans}, dominates SC permeability for moderately lipophilic solutes (Wang et al., 2007), whereas evaporative loss is directly proportional to k_g (Eqs. (16)–(17)). The multipliers were manually adjusted to match the receptor fluid (RF) kinetics for each compound, yielding the results shown in Table S2 of the SI. An independent analysis using the UB/UC model (Dancik et al., 2013) yielded substantially the same results (data not shown). Finally an optimum value of each multiplier, $\overline{\alpha}_{trans}$ and $\overline{\alpha}_{g}$, and its standard deviation were calculated as the geometric mean ± geometric dispersion of the individual α values. The optimum back-transformed values of the multipliers were $\overline{\alpha}_{trans} = 1.08$ and $\overline{\alpha}_g = 0.080$. Since the k_{trans} multiplier was very close to 1, we used the default value of k_{trans}, i.e. $\overline{\alpha}_{trans} = 1$, and the modified value of k_g, i.e. $\overline{\alpha}_g = 0.080$, in the subsequent simulations. The same correction was applied to both solute and solvent. Consequently, only a single parameter, the gas phase mass transfer coefficient k_g, was adjusted in order to produce the results shown in Section 4. The net effect was reduction of both solute and solvent evaporation rates by a factor of 12 versus default values.

Because this adjustment was made to account for conditions specific to the CE experiments, it should only be applied to experiments

conducted under identical conditions. We expect this to include the additional compounds tested in the Hewitt et al. (2019) study that are solids at skin temperature. When considering this, it is important to distinguish between supercooled liquid vapor pressure and that of the crystalline solid. The two values can be quite different, and the impact of this difference significantly impacts evaporation rates.

4. Results

4.1. Evaporated amounts

Predicted evaporation of the 18 test compounds in the CE liquids dataset is shown in Fig. 3, plotted versus that calculated as the missing radioactive dose in the IVPT study (Table 3). One compound, isoeugenol, was considered an outlier. A linear regression excluding this compound yielded.

$$\begin{aligned}(\text{Predicted evap}) &= 0.8268\,(\text{Calculated evap}) + 8.7\\ n &= 18,\ s = 10.0,\ r^2 = 0.8755\end{aligned} \tag{20}$$

A small systematic error is evident in Fig. 3, with the less volatile compounds being overpredicted and the more volatile compounds underpredicted. Nevertheless, the prediction provided by Eq. (20) was not meaningfully different from the line of perfect fit.

The evaporation and skin penetration rates of the dose solvents were not evaluated in the CE study. However, the predicted time for (nearly) complete disappearance of the solvent from the skin surface is available from the model calculations. "Nearly complete" is defined in Model 4 as less than 0.001 μg/cm^2, to avoid numerical issues associated with the size of the time steps. For PBS in bench top experiments, the calculated range was 176–210 min (n = 4). For fume hood experiments the calculated values were 92–98 min (PBS, $n = 13$), 43 min (ethanol, $n = 1$) and 7 min (acetone, $n = 1$). Most of the loss of all solvents was due to evaporation rather than penetration. The estimated residence time of water on the skin surface of 92–210 min, combined with the fact that, for the majority of compounds, most of the permeation occurred within the first 2–4 h (see Supplementary Figure S1), was the basis of choosing the fully hydrated skin option for experiments conducted using PBS dose solutions (see Section 3.2). It is likely that a simulation that allows for a gradual return to the partially hydrated skin state would yield an even better fit to the receptor fluid kinetics; however, this is not yet within our capability with Model 4.

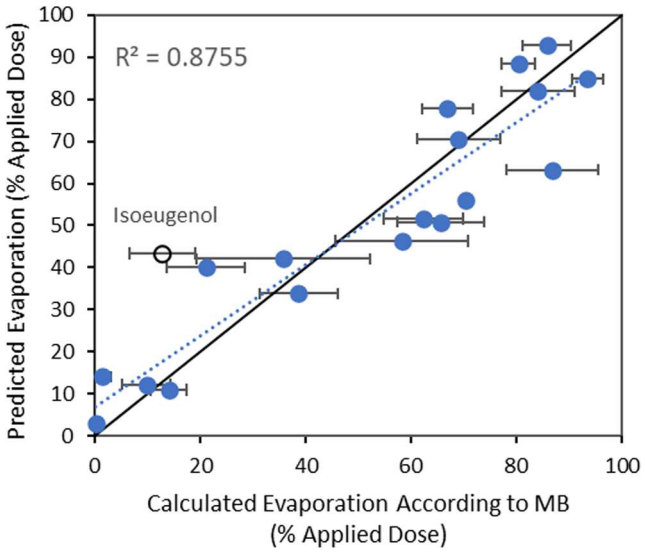

Fig. 3. Comparison of the predicted and measured evaporated fraction of 18 chemicals from the skin according to Model 4. One chemical (geraniol) was tested in two different solvents. The dotted line represents a linear regression with one outlier (isoeugenol, open circle) removed and the solid black line is the line of perfect fit.

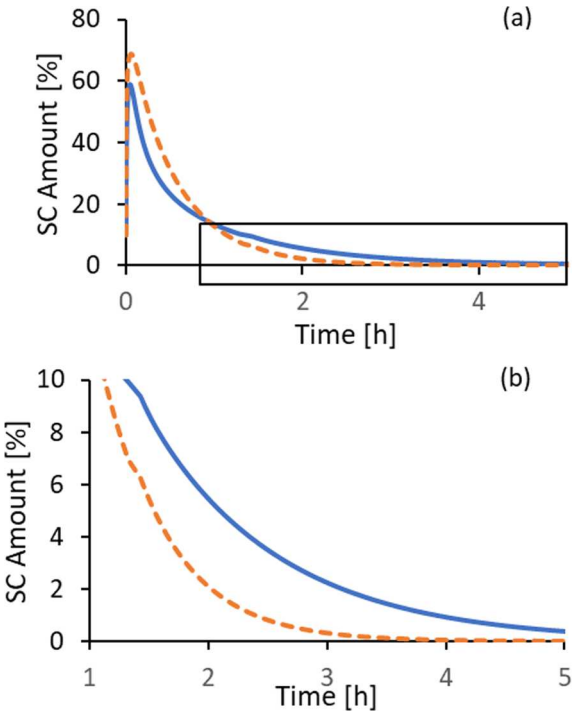

Fig. 4. (a) Predicted stratum corneum content of geraniol following topical application of 2.36 μg/cm^2 of solute in 10 μL/cm^2 of PBS solvent, expressed as a percent of applied dose. Solid blue lines reflect slowly reversible binding and orange dashes reflect equilibrium (i.e. rapidly reversible) binding. Panel (b) is a closer view of the boxed portion of Panel (a).

4.2. Impact of slowly reversible keratin binding

Fig. 4 shows the predicted amounts of geraniol in the SC as a function of time according to Model 4 in the limit of equilibrium binding and slow binding according to Eqs. (1)–(19) (solid). The values of $\overline{\overline{k}}_{on}^{sc}$ and $\overline{\overline{k}}_{off}^{sc}$ associated with the PBS simulation were 3.91×10^{-4} s^{-1} and 3.44×10^{-4} s^{-1}, respectively, and the SC permeability and partition coefficients for freely diffusing solute were $\left(P^{sc/w}\right)^{comp} = 3.18 \times 10^{-5}$ cm·s^{-1} and $\overline{\overline{K}}_{free}^{sc/w} = 11.13$, yielding $\overline{\overline{D}}^{sc} = 1.24 \times 10^{-8}$ cm^2 s^{-1} from Eq. (3). Slow binding reduces the height of the peak SC concentration, which is reached very quickly, but increases the amount of solute in the SC at times longer than about an hour. Fig. 5 shows the associated flux of geraniol into the receptor fluid (RF) and its cumulative permeation. Peak flux exiting the tissue is higher for slow binding than for equilibrium binding and is achieved a few minutes earlier. The net impact of slow binding on cumulative permeation is negligible after four hours. These observations are discussed later.

A partially hydrated skin model was used for the simulation of geraniol kinetics from ethanol (Fig. 5b). The corresponding parameter values were $\overline{\overline{k}}_{on}^{sc} = 4.16 \times 10^{-4}$s^{-1}, $\overline{\overline{k}}_{off}^{sc} = 3.44 \times 10^{-4}$s^{-1}, $\left(P^{sc/w}\right)^{comp} = 1.06 \times 10^{-5}$ cm·s^{-1}, $\overline{\overline{K}}_{free}^{sc/w} = 30.72$, and $\overline{\overline{D}}^{sc} = 4.61 \times 10^{-10}$ cm^{2}s^{-1}.

4.3. Dermal delivery and skin surface retention of test solutes

Fig. 6 shows a comparison of (a) the dermal delivery (DD) and (b) the skin surface retention of the test solutes after 24 h in the CE experiments with those predicted using Model 4. Here DD is defined as the sum of total amounts in the viable epidermis, dermis and receptor solution, as

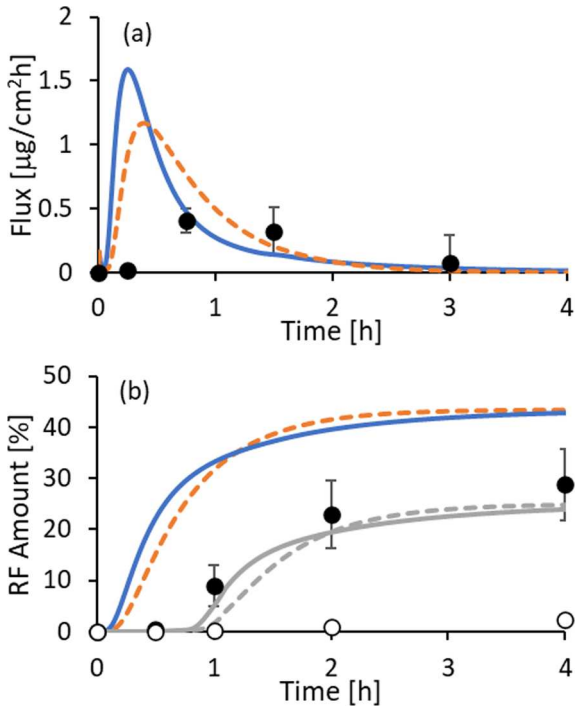

Fig. 5. Predicted (a) flux and (b) cumulative permeation of geraniol into the receptor fluid following topical application from PBS as described in Fig. 4. Solid curves denote slow binding and dashed curves denote equilibrium binding. The gray curves in Panel (b) represent the equivalent simulation results for geraniol in ethanol. Solid circles represent the CE experimental values for geraniol in PBS, whereas open circles represent the experimental values for geraniol in ethanol.

in Hewitt et al. (Hewitt et al., 2019). Skin surface retention is defined as the sum of amounts in the skin wash and stratum corneum (SC). We chose to compare the sum of the latter amounts rather than wash and SC values separately on the basis that the extensive, 8-wash procedure employed by (Hewitt et al., 2019) may have extracted some material from that retained in the SC at 24 h. The comparisons were substantially improved by this procedure.

The predicted values of DD were within two SDs of the CE data with a few notable exceptions (Fig. 6a). For all exceptions an explanation is provided. The first group are chemicals that demonstrated a high level of covalent binding to cysteine or lysine in the Direct Peptide Reactivity Assay (DPRA) (Hoffmann et al., 2022) and most likely bind irreversibly with skin proteins. This process is not currently considered within the model. The DD of three of these six compounds – benzyl bromide, 2-ethylhexyl acrylate and diethyl maleate – was substantially overpredicted. One of the overpredicted compounds, diethyleneglycol monobutylether (DEGBE), is highly water-soluble, which leads to problems with the dilute solution approximations employed in Model 4 as discussed in Section 2.4. Two others (benzyl bromide and geraniol) were dosed in acetone and ethanol, respectively. However, DD of geraniol when dosed in PBS was well predicted. DD of 4-chlorobutyric acid and thioglycolic acid, weak electrolytes dosed as salts, was overpredicted and underpredicted, respectively. The water solubility, organic solvent and weak electrolyte issues are discussed in Section 5.4.

Skin surface retention, not surprisingly, showed an inverse relationship with DD. Compounds for which DD was overpredicted had underpredicted values of material left on or near the skin surface. Notably, Model 4 predicted no skin surface retention for all compounds except for one highly water-soluble compound (DEGBE) and the four weak electrolytes. The impact of ionization of weak electrolytes on skin disposition is discussed in Section 5.4.3.

4.4. Impact of follicular delivery on dermal delivery

For the nonionizable compounds in the dataset, the Model 4 simulations indicated that the follicular pathway accounted for 0.34–11.7 % of DD, relative to a follicle-free model. The largest contributions were for methyl methane sulfonate (11.7 %) followed by acetophenone (4.15 %). These are two of the more polar compounds in the dataset.

The story was quite different for the weak electrolytes, all of which were dosed as salts. Percentage contribution of the follicular pathway ranged from 3.75 % for 4-chlorobutyric acid to 100 % for diethanolamine (DEA). The follicular contribution was related to both the ionized fraction in the SC, which was considered to retain its natural pH of 5.5, and to the degree of saturation of the dose. Highly ionized solutes did not fully penetrate the SC within the experimental timeframe, reducing the interfollicular contribution to permeation. Dilute solutes, which were preferentially distributed into the follicle during dry down, led to higher follicular permeation. Consequently, DEA (pK_a 8.71, f_{non} @ pH 5.5 = 0.0006) had the highest follicular contribution to permeation – essentially 100 % of DD. However, the total DD for DEA in the *presence* of follicles was only 1.49 % of the initial dose. From a risk assessment perspective, the contribution was small. All other compounds in the dataset had lower absolute follicular delivery percentages than DEA.

Details of the follicular delivery contribution for each compound may be found in Table S5 in the SI.

4.5. Receptor fluid kinetics

Plots of the predicted receptor fluid kinetics of each compound are shown in Supplementary Figure S1. They correspond closely with the DD results in Fig. 6a, as both experimental and predicted DD values are dominated by the 24 h receptor fluid amount.

5. Discussion

A substantial effort was put into correctly representing these experiments in simulations, especially evaporation and ionization. This experience provides learning regarding the importance of carefully considering the experimental conditions to correctly predict skin disposition and cautions against using model values calibrated for default conditions.

5.1. Evaporative loss from skin

Predicted percent of dose evaporated (%Evap) was in good agreement with the values observed in the experiments, calculated as 100 % − MB, once the average mass transfer coefficient, k_g, was multiplied by a factor of $\alpha_g = 0.080$ (Fig. 3). As is evident from Eq. (18), it is not possible to determine which factor, or combination of factors, comprising k_g was responsible for the overestimate provided by the default model without additional information. (Hamadeh et al., 2021) made a similar correction by substantially lowering the wind velocity (or air flow), u, in order to lower evaporation of a closely related subset of the CE data. We note that the structure of k_g including the exponent associated with u are sensitive features of the geometry of the evaporating surface and the nature of the surrounding airstream. Fig. 7 shows the variety of Franz cell tops available in our laboratory. The cells employed in the calibration of the UB/UC model used tops that were similar to the leftmost image, but were erroneously reported to be even shorter (4 mm) (Gajjar et al., 2013), as confirmed recently by photographs supplied by Dr. Gajjar. They were placed in an aluminum block within a heating/stirring module and protruded about 4 cm above the surface of the module. The module was placed either on the benchtop or in the full airflow of a fume hood with the sash at 46 cm (18″), a velocity estimated to be 0.874 $m \cdot s^{-1}$, as described in (Gajjar et al., 2013). The CE study employed Bronaugh-type cells with a height of 14 mm above the skin surface (similar to the middle picture in Fig. 7) and with mounting screws

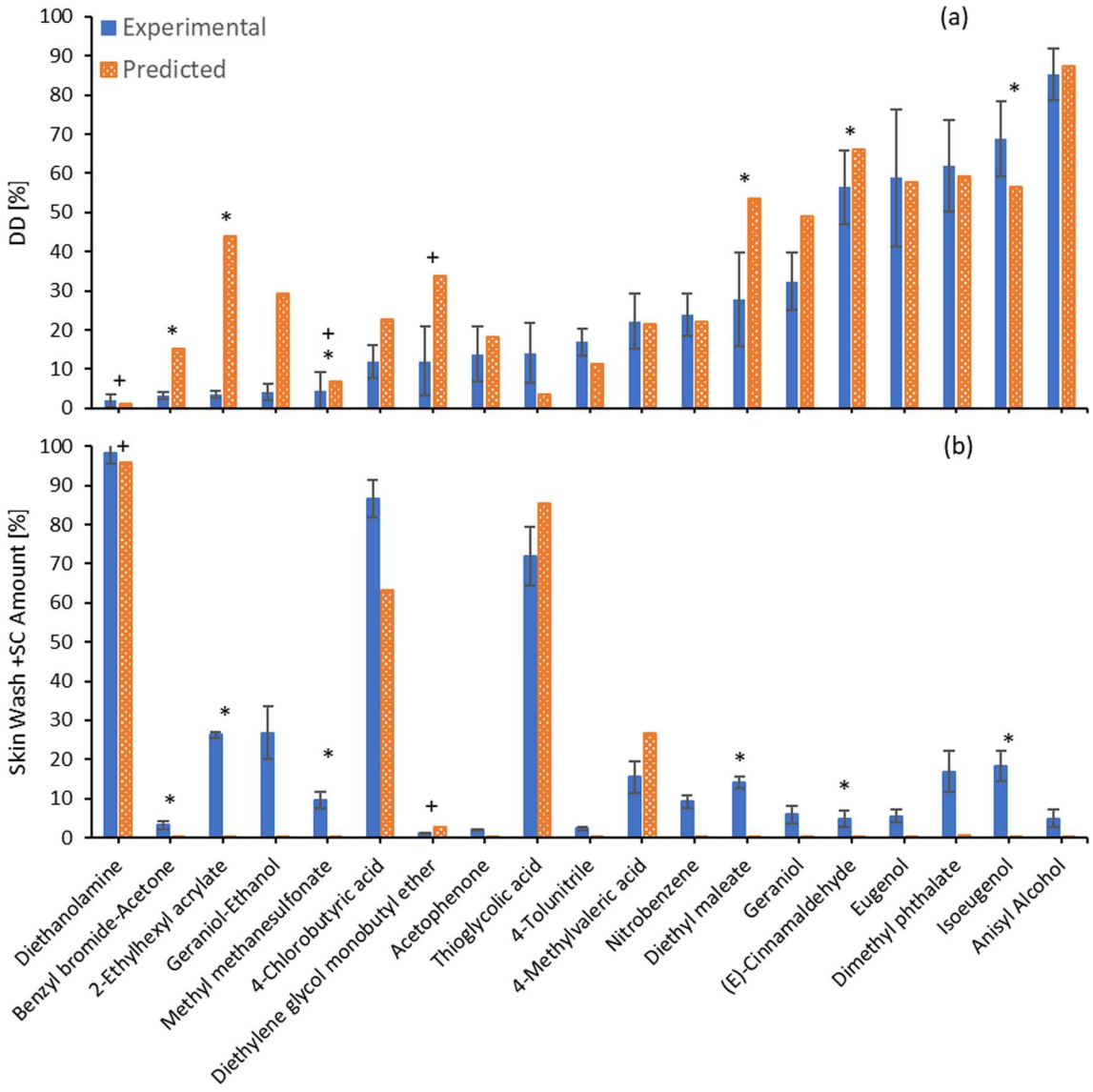

Fig. 6. Comparison of skin disposition after 24 h for CE liquids dataset (solid blue) and simulated results using Model 4 (orange pattern). (a) Dermal delivery (ED + DE + receptor fluid); (b) Skin wash + SC. A "*" indicates a compound that covalently binds to CYS or LYS leading to depletion ≥ 30 %. A "+" indicates a compound with high water solubility. Error bars reflect the standard deviation of the summed values.

Fig. 7. Low-, medium- and high-top Franz diffusion cell caps available in our laboratories (GBK, LX). The caps used to calibrate the UB/UC model were similar to the leftmost picture. The caps used in the CE study (Hewitt et al., 2019) had approximately the same height as the top in the middle picture, but also a different design and mounting configuration as described in the text.

impeding the airflow from two sides of the apparatus (Emilie Raynaud, DMPK Project Manager, Eurofins I ADME Bioanalyses, personal communication). Orientation and airflow over the apparatus are not stated in (Hewitt et al., 2019) and were not available from Dr. Raynaud. Thus, there are significant differences between the CE study and the calibration study embodied in UB/UC. In our estimation, these differences may account for the overestimation of evaporation rates in the CE study by the default UB/UC and Model 4 models.

In the analysis described herein, we have employed the same evaporation mass transfer model for solute and solvent, i.e. one employing a 12-fold lower gas phase mass transfer coefficient than that recommended in (Dancik et al., 2013). This choice implies that both aqueous and organic solvents are present on the skin surface (or in a swollen SC) for substantial periods of time, as described in Section 4.1. The fact that water in the PBS donor solution is present in the simulation for 1.5–3 h is the basis for choosing a hydrated skin model for experiments involving PBS. We note that there were neither direct or indirect measurements of solvent evaporation rate in (Hewitt et al., 2019) although several factors related to evaporation such as ambient temperature and relative humidity were controlled. The well controlled experimental conditions

allow the assumption that the same adjustment to the mass transfer coefficient would be appropriate throughout the dataset and the solvent evaporation rate can be estimated despite not being directly measured.

This assumption is very different from the one employed by (Hamadeh et al., 2021), who allowed the solvent evaporation rate to vary independently of the solute evaporation rate. By allowing the solvent to evaporate quickly, but the solutes to evaporate slowly, and simultaneously reducing the thickness of the SC deposition zone, they were able to improve model predictions for the full CE finite dose dataset. As an example of how different the solvent evaporation rate assumptions are, Hamadeh's Model B evaporation rate constant for PBS in Table 3 yields complete evaporation of water in 1.8 min, regardless of environment, whereas the modified Model 4 in the present analysis places this value at 174–178 min (bench top) and 85–86 min (fume hood), as noted in Section 4.1. The difference is stark. The Model 4 analysis suggests that distribution of the residual solvent between the skin surface and the SC during the dry down period led to skin permeability consistent with fully hydrated skin for the first several hours post-dose.

We understand the advantage obtained in fitting the CE solids data with a rapid solvent evaporation and small deposition zone approach, as significant amounts of solids deposited on the skin surface in the CE study. However, in our view, it is inconsistent from a physics perspective to employ different evaporation models for solute and solvent. In the present analysis we obtained a reasonable model of the CE liquids data without employing either of these approximations. Solute evaporation was adequately simulated by reducing the evaporation mass transfer coefficient and slowly reversible binding accounted for the reduction in deposition zone capacity for the dataset analyzed herein.

The inclusion of thermodynamic activities, a_i, for both solute and solvent in Eq. (16) further differentiates the evaporative loss model described here from that employed by (Hamadeh et al., 2021). These workers assumed constant evaporation rates for both components for as long as they were present on the skin surface, whereas evaporation rates in Model 4 evolve with the activities of both solute and solvent, which are functions of solution composition and ionization state of the solute.

5.2. Slowly reversible binding

Solute partitioning and diffusion in the SC in Model 4 is substantially different from UB/UC or earlier versions of the gPROMS model. Slowly reversible binding to keratin changes the kinetics of the permeating species. If the binding on/off rate is very slow compared to the diffusion rate, the solute will initially diffuse as if none binds to keratin. The apparent lag time for solute exiting the SC and later the skin is thus shorter for compounds that bind slowly, cf. Fig. 5b. And yet, according to the present parameterization, cumulative permeation after several hours is not meaningfully different from the same solute undergoing rapidly reversible (i.e. equilibrium) binding. This parameterization also restricts significant impact of slow binding to highly lipophilic compounds (e.g. $\log K^{ow} > 3.5$, similar to geraniol) that have very low on and off rates. The calculations below suggest two ways of quantitatively understanding these phenomena.

The values of $\bar{\bar{k}}_{on}^{sc}$ and $\bar{\bar{k}}_{off}^{sc}$ associated with the geraniol/PBS simulation in Figs. 4 and 5 (see Section 4.2), combined with the conventional model for reversible binding in the absence of transport, lead to an effective time constant for binding in the SC of

$$\tau_B = \left(\bar{\bar{k}}_{on}^{sc} + \bar{\bar{k}}_{off}^{sc}\right)^{-1} = 1361 \text{ s or } 0.38 \text{ h} \quad (21)$$

This value may be compared with the diffusive time constant for freely diffusing solute in the SC,

$$\tau_D = \frac{(h^{sc})^2}{\bar{\bar{D}}^{sc}} = \frac{(0.00434\text{cm})^2}{1.24 \times 10^{-8}\text{cm}^2\text{s}^{-1}} = 1519 \text{ s or } 0.422 \text{ h} \quad (22)$$

Here, the values of h^{sc} and $\bar{\bar{D}}^{sc}$ are taken from Table 1 and Section 4.2, respectively. This comparison indicates, for geraniol ($\log K^{o/w} = 3.56$) permeating through hydrated SC according to the Seif and Hansen calibration (Eq. (7)), slow binding and diffusion have comparable time scales. The simulation in Figs. 4 and 5 shows that the SC kinetics and time lag are appreciably altered from the equilibrium binding case, but the ultimate disposition of the compound following topical application is not. The latter finding applies also to the other, less lipophilic compounds in this dataset (see Supplementary Fig. S1).

In the case of an infinite dose and very slow binding, the observed lag time for solute exiting the SC will approach $\tau_D/6 = 253$ s or 0.070 h. Less obvious is the observation that the apparent lag time of a finite dose also approaches this value. A close examination of Fig. 5b provides a supporting example. We find this to be also true for equilibrium binding. The corresponding time lag in this case is 0.150 h, based on an equilibrium diffusivity of $D_{eq}^{sc} = 5.80 \times 10^{-9}$ cm^2 s^{-1}, calculated as $\bar{\bar{D}}^{SC}/(1 + \bar{\bar{k}}_{on}^{ker}/\bar{\bar{k}}_{off}^{ker})$. For a comparison, see Frasch et al's Eq. (3) (Frasch et al., 2011).

A parallel calculation for geraniol in partially hydrated skin (ethanol dose solvent – Fig. 5b) yielded $\tau_B = 0.37$ h, $\tau_D = 1.08$ h, and lag times of 0.18 h and 0.40 h, respectively, for slow binding and equilibrium binding approximations. However, another factor comes into play in the simulations, leading to effective lag times of about 0.8–1.0 h. Geraniol is very soluble in ethanol, and the dose solutions as initially prepared had low geraniol activity (calculated as fraction of solubility), lowering its ability to partition into the skin. The estimated residence time of ethanol on the skin in the fume hood environment in the Model 4 simulation was 31 min (Section 4.1). Consequently, the simulated penetration of geraniol into the skin and its eventual exit from the skin were delayed by the presence of residual solvent.

5.3. Impact of follicular delivery plus slow binding on experimental time lags

As discussed in the preceding section, slow binding introduces a second time constant into SC permeation kinetics which can be of the same order of magnitude as the diffusive time constant. The binding effect leads to an apparent SC diffusivity that changes with time. Follicular delivery (cf. Section 4.4) introduces yet another time scale for permeation that is generally faster than that of the composite SC. The combination of the two diffusive processes plus a slow binding equilibrium yields complex permeation transients not describable by a single lag time or diffusion coefficient. This would be true even in an infinite dose penetration experiment where skin permeability coefficient, k_p, is derived from the steady-state flux. In a finite dose experiment, the time lag is further impacted by solvent dry down as discussed in Section 5.2. The value of k_p is not sensitive to the various time constants in the system, but the time lag τ to achievement of steady state is. Thus, the inference of an effective diffusivity D_{sc} from the relationship $D_{sc} = {h_{sc}}^2/6\tau$ is problematical and may be misleading. The system cannot be homogenized to yield a diffusive system with a single time constant unless one of the three processes dominates the kinetics.

5.4. Dermal delivery and skin surface retention

DD and skin surface retention of CE liquids were reasonably well predicted by Model 4, with the exceptions noted in Section 4.3. This section will focus on these exceptions. They fall into three classes: peptide-reactive compounds, highly water-soluble compounds and weak electrolytes.

5.4.1. Peptide-reactive compounds

Six of the compounds in the 18-compound CE liquids dataset are highly reactive with either cysteine or lysine in the DPRA assay

(Hoffmann et al., 2022; Jaworska et al., 2015), or the DPRA-equivalent leg of kDPRA, a kinetic version of DPRA involving cysteine only (Natsch et al., 2020), as indicated in Fig. 6 and tabulated in Supplementary Table S3. All of these compounds have maximum kDPRA rate constants near or above the published cutoff value of log $k_{max} \geq -2.0$ for distinguishing between GHS Cat 1A and GHS Cat 1B sensitizers (Wareing et al., 2020b) (Table S4). Here, the units of k_{max} are $s^{-1}M^{-1}$. Model 4 overpredicted the DD of three of these compounds. It is quite likely that covalent binding to SC proteins accounts for a good part of the discrepancy for the peptide-reactive compounds, as chemical reactivity is not included in Model 4 or its predecessors. As an example of how it might be taken into account, Fig. 8 shows a comparison of Model 4 predictions with kDPRA rate constants. Prediction accuracy, expressed as DD(predicted)/DD (observed), hovers around unity for $k_{max} \leq 0.05$, corresponding to log $k_{max} = -1.3$. This value lies between the originally published cut-off of log $k_{max} \geq -1.1$ (Wareing et al., 2020a) and the refined cut-off of log $k_{max} \geq -2.0$. One compound, 2-ethylhexyl acrylate (EHA), was over-predicted by an order of magnitude. EHA had a high cysteine depletion in DPRA (98.8 %), but only a moderate kDPRA rate constant (log $k_{max} = -2.13$). Further investigation reveals that EHA is highly reactive according to the refined Peroxidase Peptide Reactivity Assay (PPRA), showing direct reactivity with cysteine with a lowest EC25 value of only 0.017 mM (Ryan et al., 2020). Thus, the published kDPRA rate constant does not reflect the full extent of its peptide reactivity.

5.4.2. Highly water-soluble compounds

The highly water-soluble compounds were diethanolamine (DEA), methyl methane sulfonate (MMS) and diethylene glycol monobutyl ether (DEGBE). DEA is also a weak electrolyte and was adequately handled by Model 4; it will be discussed in the context of ionization. MMS is cysteine-reactive (Figs. 6 and 8) but was well handled once the concentration limitation discussed in Section 2.4. was enforced. DEGBE, also known as 2-(2-butoxyethoxy)ethanol and butyl carbitol, is a widely used, water-miscible solvent, similar to other low molecular weight glycol ethers including the paint solvent 2-butoxyethanol (BE). The penetration of BE in human, guinea pig and rat skin, and also silicone membrane, has been carefully characterized (Bunge et al., 2012). In each case it was found to be highly nonlinear with respect to aqueous concentration, due in part to nonideal solution thermodynamics. Activity-normalized flux of BE through silicone membrane was found to be constant, whereas the same normalized flux through skin decreased with BE concentration. This variation was attributed to a decrease in skin hydration at high BE concentrations. We postulate that aqueous DEGBE solutions share properties similar to aqueous BE. Evaporation of DEGBE at low concentrations is likely to be faster than Model 4 predictions due to high thermodynamic activity, whereas skin penetration at high concentrations may be lower than predictions due to a decrease in skin hydration. These factors complicate accurate modeling of DEGBE permeation through skin.

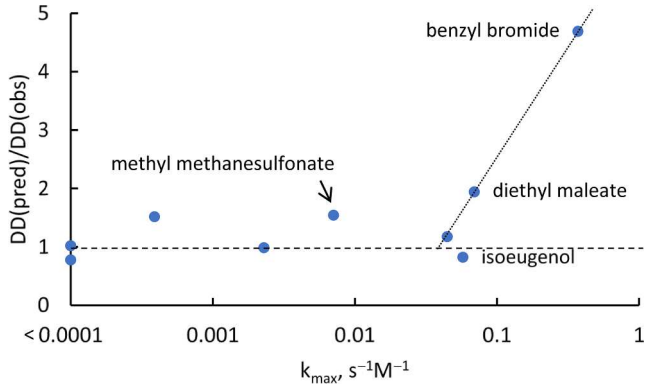

Fig. 8. Ratio of Model 4-predicted to observed dermal delivery for cysteine-reactive compounds in CE liquids dataset plotted versus k_{max} value in kDPRA assay (Wareing et al., 2020a). The dashed line is the line of perfect fit. Dotted line indicates plausible influence of cysteine reactivity. Outlying values are discussed in the text. An additional outlying compound, 2-ethylhexyl acrylate, with a highly overpredicted DD but moderate k_{max} value is not shown.

Other highly water-soluble compounds in the CE study were the two organic solvents, ethanol and acetone. Although the skin disposition of the dose solvents (including water) was not measured, it is a key element of the Model 4 simulations for the associated solutes. Accurate modeling of the organic solvents presents some of the same issues as those for DEGBE. In particular, the assumption of a constant SC/water partition coefficient equal to the dilute solution value (the Model 4 default) fails for these compounds and leads to unreasonably high SC concentrations. We overcome this issue by limiting the solvent and solute concentrations in the SC as discussed in Sects. 2.2 and 2.4. This approach yields plausible values for skin permeation, but it lacks the rigor of a mechanistic solution to the problem.

5.4.3. Weak electrolytes

Four of the compounds in the CE liquids dataset were weak electrolytes – DEA, TGA, 4-chlorobutyric acid (CBA) and 4-methylvaleric acid (MVA). DEA is a weak base (pK_a 8.71); the other three are weak acids with pK_a values in the range 3.7–4.8 (Table 2). They were applied to the skin at specific doses of 10–72 μg/cm^2 in PBS solutions having initial pH values of 6.0–7.0 (Table 3). Thus, all four compounds were highly ionized in the dose solutions. The molar equivalents of the specific doses range from 97 to 787 nmol/cm^2.

Recent work in our laboratory, using a representative weak acid and weak base applied to skin in finite doses, has established the effective buffer capacity of skin to neutralize solvent-deposited weak electrolytes is in the range 10–20 nmol/cm^2 (Miller and Kasting, 2022). The above compounds were all applied in ionized form at doses well above this range, essentially ensuring the SC would not substantially buffer the pH during dry down and the solute deposited upon evaporation would be largely in the form of a salt. In fact, the considerable evaporative loss for MVA and small loss for TGA during dry down would drive the pH of these solutions and the degree of ionization higher, as the evaporating species is the free acid. Considering the composition of the solution, the deposited solutes would be chloride and phosphate salts of DEA and sodium salts of the three weak acids. All are expected to be solids at skin temperature. Consequently, these CE "liquids" most likely behaved as dissolved solids in the skin penetration study and penetrated poorly both before (as ionized solutes) and after (as deposited solids) evaporation of the solvent.

In the simulations, we treated the weak electrolytes as "hard solids" after dry down of the dose solution, i.e. partitioning of the deposited solid into the skin was not allowed. This is the same approximation employed by (Hamadeh et al., 2021) and was effective in obtaining a good fit to the data. It is not always appropriate, however, as we have shown elsewhere (Kasting et al., 2022; Yu et al., 2022). Neither is it completely accurate for the weak electrolytes in the present analysis, as may be seen from the slow accumulation of each compound in the receptor fluid at times up to 24 h evident in Supplementary Fig. S1.

5.4.4. Solvent effects

Hewitt et al. established, for three of four compounds tested, that skin permeation from PBS was substantially higher than that from ethanol (Hewitt et al., 2019). The doses employed were the same as those in the larger study, which ranged from 1.0 to 5.4 μg/cm^2 for these four compounds. Only one of these compounds, geraniol, is a liquid at skin temperature. Fig. 5b shows that Model 4 can account for some of the difference in the geraniol results in the two solvents, based on the choice of the skin hydration state as discussed in Sects. 4.1 and 4.2., but the agreement is incomplete.

Organic solvents have been employed for many years in finite dose skin penetration experiments without apparent issues in topical delivery

– see, for example, (Feldmann and Maibach, 1970; Feldmann and Maibach, 1974; Scheuplein and Ross, 1974). Li and coworkers made direct comparisons of the human skin permeation of corticosterone (Intarakumhaeng and Li, 2014) and five other compounds (Intarakumhaeng et al., 2018) after finite dosing of tracer levels from a variety of solvents. In only one of the cases (estradiol) was water the best delivery solvent. We note that one of the two compounds dosed in organic solvents in the present analysis of CE liquids, benzyl bromide, is highly peptide-reactive, which complicates interpretation of the results.

Net, we don't have a full explanation of solvent effects in the present dataset. The rapid solvent evaporation explanation offered by Hamadeh et al. (Hamadeh et al., 2021) doesn't work well for geraniol, which will deposit as a liquid in the absence of chemical degradation and still be available for penetration. We defer a more complete analysis to a later effort involving more experimental data.

6. Conclusions

The present study was conceived as an effort to determine the ability of our evolving computational model to simulate human skin permeation of small doses of cosmetically-relevant compounds as measured in an in vitro study (Hewitt et al., 2019). A substantial effort was put into correctly representing these experiments in simulations, especially evaporation and ionization. The effort provides learning on the importance of carefully considering the experimental conditions to correctly predict skin disposition and cautions against simply using values calibrated for default conditions. We successfully explained dermal delivery (primarily skin permeation) of the chosen experimental set and provided an explanation for the outliers that are outside the scope of the current model. The advances achieved in the model make it a better tool for predicting dermal absorption than were earlier versions.

Model 4 incorporated recently developed features that had not been thoroughly tested, including a polar pathway through the stratum corneum (SC), slowly reversible keratin binding of permeants diffusing in the SC, dry down of solutions of potentially volatile and/or ionizable solutes in a volatile solvent, and a revised limitation on the partitioning and diffusivity of highly water-soluble permeants within the SC. The polar pathway feature was not particularly influential for the non-ionizable compounds in the analyzed dataset, as similar skin permeation rates and distributions could be obtained with the older UB/UC model, elsewhere called Dancik et al. (Hamadeh et al., 2021) and CDC (Gregoire et al., 2021). However, when combined with the concept of precipitation of salts during dry down, it did offer an improved explanation for the permeation and distribution of weak electrolytes applied to skin in their ionized form. Accounting for simultaneous evaporation of solute and solvent with evaporation rates varying in time according to vehicle thermodynamics yielded a good explanation of experimental data.

Slowly reversible keratin binding, as presently parameterized, did not appreciably change the ultimate disposition of compounds in the analyzed dataset. But it did alter the kinetics of lipophilic solute entry into and exit from the SC, as well as their effective time lags for permeation into the receptor fluid. Since appendageal diffusion can also alter the time lag of hydrophilic solutes, the combination of these two features (slow binding and appendageal diffusion) explains why it has proven problematical to estimate SC diffusion coefficients from time lags observed in IVPT studies. In many cases transient transport in the SC simply cannot be described by a single diffusivity or associated time constant.

The analysis points to several features that must be carefully considered when designing and interpreting IVPT studies of potentially volatile and chemically reactive compounds: (1) evaporation rates of both solute and solvent depend on the design of the diffusion cells and their location in the laboratory or fume hood, as well as skin surface and laboratory temperatures. The use of a default evaporation model based on conditions other than those employed can lead to erroneous results; (2) skin permeation and tissue distribution of chemically reactive compounds, or those that otherwise bind irreversibly to skin components are outside the scope of the current model that does not incorporate these features; (3) topical application of weak electrolyte solutions buffered at a pH values different from their intended use in products is likely to yield poor predictions of consumer exposure. Model 4 offers a chance to correct experimental data for moderate changes in formulation pH.

7. Recommendations

7.1. Evaporative loss

For experimental IVPT studies in which evaporation is an important component, we advise that workers calibrate their equipment with one or more standard volatile compounds. We offer the gravimetric method employed by (Gajjar et al., 2013) as an example; however, more precise or efficient methods are certainly possible, cf. (Frasch et al., 2018). Bear in mind that even location in the laboratory or fume hood may influence evaporation rates unless care is taken to ensure uniform air flow over the apparatus. Evidence of this is the variability in the evaporative loss in the present dataset (Fig. 3). Some guidance may be obtained from simpler experiments such as the pre-test evaporation experiments conducted by (Gregoire et al., 2019); however, a correlation with IVPT evaporation rates must be established. Accurate measurements of vapor pressure are also important to enable accurate estimates of evaporation rates, as shown by Eq. (17). We note that the accuracy of vapor pressure estimates tabulated in sources such as EpiSuite™ (US_EPA, 2011) depends upon the amount and type of available input data, which is often quite limited for complex chemicals.

For simulation of evaporation there is a rich literature upon which to draw. For a short but thoughtful review of this area and suggestions for improvements in calculating evaporation from skin, we recommend (Frasch and Bunge, 2015) and (Frasch et al., 2018). For details on the inverse process, i.e. dermal uptake of vapors from the atmosphere, we note the work of Morrison and coworkers, e.g. (Morrison et al., 2016), who have modeled semi-volatile organic compound (SVOC) uptake into human skin in vivo in a series of exposure chamber studies. The mass transfer coefficients estimated therein should be adaptable to the skin evaporation problem. Finally, we note that in the limit of very low external airflow, unforced (natural) convection due to thermal gradients dominates the evaporation process and very different mass transfer relationships apply (Bird et al., 2002). These relationships are highly sensitive to the geometry of the system and to the temperature gradient. This area is ripe for thoughtful reapplication of off-the-shelf technology.

7.2. Chemical reactivity

Possible chemical reactions between permeant and skin include, but are not limited to, oxidation on the skin surface, hydrolytic degradation in the vehicle or tissue and covalent binding to skin components. Covering all this ground is no simple task. For cosmetic and personal care products, the DPRA database and associated analyses thereof, e.g. (Jaworska et al., 2015), provide a starting point for reaction of permeating solutes with skin proteins. A modest number of kDPRA maximum rate constants, k_{max}, are also available (Roberts et al., 2008; Roberts and Natsch, 2009; Wareing et al., 2020a), as are broader chemical reactivity discussions related to skin sensitization (Chipinda et al., 2014; Schwobel et al., 2011). Fig. 8 suggests the potential of utilizing k_{max} values in the reactivity calculation. Building a framework for these reactions into simulation models is an important step toward modeling the disposition of known and potential skin sensitizers.

7.3. Highly water-soluble compounds

If dissolved in a more volatile solvent these compounds will concentrate on the skin surface during dry down of an aqueous

formulation. Diffusion in concentrated solutions is inherently more complex than that in dilute solutions due to coupling between components, and partition relationships with neighboring media are also impacted (Cussler, 1997). Furthermore, some highly soluble solutes have very non ideal thermodynamic activities in aqueous solution, e.g. 2-butoxyethanol (Bunge et al., 2012), 2-hydroxypropyl acrylate (Frasch et al., 2014) and niacinamide (Charman et al., 1991; Yu et al., 2022). Consequently, they do not adhere to dilute solution partition relationships and require special attention when modeling transport in skin. Improved methods of handling these compounds are needed.

7.4. Underlying skin permeability model

For the compounds in the present dataset, the diffusive resistance of the SC dominates the skin barrier. According to the underlying SC permeability model (Wang et al., 2006, 2007), as modified for highly polar solutes (Kasting et al., 2019), transverse diffusion across SC intercellular lipids is the rate-limiting step for all but very hydrophilic or very lipophilic compounds. Transverse diffusivity across the lipids, in turn, is estimated by a mass transfer coefficient, k_{trans}, multiplied by the lipid bilayer width δ. The value of k_{trans} is presently calculated from molecular weight and skin hydration state only, again with a small leakage pathway for highly polar solutes. We infer from the present and other analyses that more molecule-specific information is required to significantly improve estimates of k_{trans} or closely-related parameters, which might additionally include diffusive resistance of the cornified cell envelope (Schwobel et al., 2020). This would be an excellent area to incorporate information from molecular, coarse-grain or quasi-quantum modeling.

CRediT authorship contribution statement

Kevin Tonnis: Investigation, Formal analysis, Visualization, Writing – original draft. **Johannes M. Nitsche:** Funding acquisition, Formal analysis. **Lijing Xu:** Investigation, Formal analysis. **Alison Haley:** Visualization, Validation. **Joanna Jaworska:** Funding acquisition, Supervision, Formal analysis. **Gerald B. Kasting:** Funding acquisition, Supervision, Formal analysis, Writing – review & editing.

Declaration of Competing Interest

The authors declare that they have no known competing financial interests or personal relationships that could have appeared to influence the work reported in this paper.

Data availability

Algorithms are fully described in this article and its predecessors. Computational results are available in the Supplemental Information. The gPROMS computer code is the property of Procter & Gamble.

Acknowledgments

KT and AH were supported by the Procter & Gamble Company. LX, JMN and GBK were supported by a grant from the US National Science Foundation (NSF) GOALI program under grant numbers 2124495 and 2124542 (CBET).

Appendix A

For precise calculations, the formula for partitioning of free solute in the corneocyte phase of the SC given in Eq. (6) should be replaced by a form accounting for steric exclusion of the solute from an annular ring of solvent surrounding the perimeter of the keratin microfibrils. The correction was developed in (Wang et al., 2007) and later employed by (Nitsche and Kasting, 2022). For a spherical solute having a hydrodynamic radius a^{solute}, the appropriate correction is.

$$\overline{K}_{free}^{cor/w} = \left[1 - \phi^{ker}(1+\lambda)^2\right] \Big/ \left(f_{non}^{cor}\right)_{free} \tag{A1}$$

where $\lambda = a^{solute}/a^{ker} = a^{solute}/35$ Å. For the same reason, Eq. (10) must also be modified for finite-sized solutes. The appropriate modification is (Nitsche and Kasting, 2022):

$$\overline{\overline{k}}_{on}^{sc} = k_{on}^{ker} \cdot \left(\frac{(\rho^{ker}/\rho^{w})\phi^{ker}}{\left(f_{non}^{cor}\right)_{free}\left(\overline{\phi}^{lip}/\overline{\phi}^{cor}\right)\overline{K}^{lip/w} + 1 - \phi^{ker}(1+\lambda)^2} \right) \tag{A2}$$

Values of the constants $\phi^{ker}, \rho^{ker}, \overline{\phi}^{lip}$ and $\overline{\phi}^{cor}$ for fully and partially hydrated skin are given in Table 1. Versions of these equations for nonionizable solutes with numerical values inserted may be found in (Wang et al., 2007) (Eq. A(1)) and (Nitsche and Kasting, 2022) (Eqs. A(1) and A(2)).

Suitable estimates for molar volume, V_A, for small molecules at their normal boiling points can be developed from Schröder's Method (Poling et al., 2001), as recommended in (Wang et al., 2007). These estimates can be simply converted to hydrodynamic radii, a^{solute}, by Eqs. (B5) in (Wang et al., 2007), included here for clarity:

$$a^{solute} = (0.156\,\text{Å})(V_A)^{0.6} \quad \text{for } V_A \leq 334.5 \quad \text{cm}^3/\text{mol} \tag{A3a}$$

$$a^{solute} = (0.735\,\text{Å})(V_A)^{1/3} \quad \text{for} \quad V_A > 334.5 \quad \text{cm}^3/\text{mol} \tag{A3b}$$

Molar volume estimates from computational chemistry sources or approximate relationships between V_A and molecular weight (Ibrahim et al., 2012) can also be employed. For small molecules one must ensure that the selected value of V_A is consistent with diffusivities derived from the Wilke-Chang equation (Wilke and Chang, 1955) with the correction to the association constant for water suggested by (Hayduk and Laudie, 1974), which are embodied in Eq. (A3a). Because hydrodynamic radii also play a key role in diffusivity estimates within the skin in the UB/UC model or extensions thereof, it is important to choose a method wisely and to maintain the same value of a^{solute} throughout the model calculation in order to obtain self-consistent results.

Appendix B. Supplementary information

Supplementary data to this article can be found online at https://doi.org/10.1016/j.ijpharm.2022.122030.

References

Anissimov, Y.G., Roberts, M.S., 2004. Diffusion modeling of percutaneous absorption kinetics: 3. Variable diffusion and partition coefficients, consequences for stratum corneum depth profiles and desorption kinetics. J. Pharm. Sci. 93 (2), 470–487.

Anissimov, Y.G., Roberts, M.S., 2009. Diffusion modelling of percutaneous absorption kinetics: 4. Effects of a slow equilibration process within stratum corneum on absorption and desorption kinetics. J. Pharm. Sci. 98 (2), 772–781.

Basketter, D.A., Pease, C., Kasting, G.B., Kimber, I., Casati, S., Cronin, M.T.D., Diembeck, W., Gerberick, G.F., Hadgraft, J., Hartung, T., Marty, J.P., Nikolaidis, E., Patlewicz, G.Y., Roberts, D., Roggen, E., Rovida, C., van de Sandt, H., 2007. Skin sensitisation and epidermal disposition. The relevance of epidermal bioavailability for sensitisation hazard identification/risk assessment. ATLA 35, 137–154.

Berner, B., Juang, R.-H., Mazzenga, G.C., 1989. Ethanol and water sorption into stratum corneum and model systems. J. Pharm. Sci. 78 (6), 472–476.

Bird, R.B., Stewart, W.E., Lightfoot, E.N., 2002. Transport Phenomena, 2nd ed. Wiley, New York, Sect. 11-3 and 11-4.

Bunge, A.L., Persichetti, J.M., Payan, J.P., 2012. Explaining skin permeation of 2-butoxyethanol from neat and aqueous solutions. Int. J. Pharm. 435 (1), 50–62.

Charman, W.N., Lai, C.S.C., Finnin, B.C., Reed, B.L., 1991. Self-association of nicotinamide in aqueous solution: mass transport, freezing-point depression, and partition coefficient studies. Pharm. Res. 8, 1144–1150.

Chipinda, I., Mbiya, W., Adigun, R.A., Morakinyo, M.K., Law, B.F., Simoyi, R.H., Siegel, P.D., 2014. Pyridoxylamine reactivity kinetics as an amine based nucleophile for screening electrophilic dermal sensitizers. Toxicol. 315, 102–109.

Cussler, E.L., 1997. Diffusion: Mass Transfer in Fluid Systems, 2nd ed. Cambridge University Press, Cambridge.

Dancik, Y., Miller, M.A., Jaworska, J., Kasting, G.B., 2013. Design and performance of a spreadsheet-based model for estimating bioavailability of chemicals from dermal exposure. Adv. Drug Deliv. Revs. 65 (2), 221–236.

Ellison, C.A., Tankersley, K.O., Obringer, C.M., Carr, G.J., Manwaring, J., Rothe, H., Duplan, H., Géniès, C., Grégoire, S., Hewitt, N.J., Jamin, C.J., Klaric, M., Lange, D., Rolaki, A., Schepky, A., 2020. Partition coefficient and diffusion coefficient determinations of 50 compounds in human intact skin, isolated skin layers and isolated stratum corneum lipids. Toxicol. In Vitro 69, 104990.

Feldmann, R.J., Maibach, H.I., 1970. Absorption of some organic compounds through the skin in man. J. Invest. Dermatol. 54 (5), 399–404.

Feldmann, R.J., Maibach, H.I., 1974. Percutaneous penetration of some pesticides and herbicides in man. Toxicol. Appl. Pharmacol. 28 (1), 126–132.

Fluhr, J.W., Elias, P.M., 2002. Stratum corneum pH: formation and function of the acid mantle. Exog. Dermatol. 1, 163–175.

Frasch, H.F., Barbero, A.M., Hettick, J.M., Nitsche, J.M., 2011. Tissue binding affects the kinetics of theophylline diffusion through the stratum corneum barrier layer of skin. J. Pharm. Sci. 100 (7), 2989–2995.

Frasch, H.F., Barbero, A.M., Dotson, G.S., Bunge, A.L., 2014. Dermal permeation of 2-hydroxypropyl acrylate, a model water-miscible compound: effects of concentration, thermodynamic activity and skin hydration. Int. J. Pharm. 460 (1-2), 240–247.

Frasch, H.F., Bunge, A.L., 2015. The transient dermal exposure II: post-exposure absorption and evaporation of volatile compounds. J. Pharm. Sci. 104 (4), 1499–1507.

Frasch, H.F., Lee, L., Barbero, A.M., 2018. Spectral reflectance measurement of evaporating chemical films: initial results and application to skin permeation. J. Pharm. Sci. 107 (8), 2251–2258.

Gajjar, R.M., Miller, M.A., Kasting, G.B., 2013. Evaporation of volatile organic compounds from human skin in vitro. Ann. Occup. Hyg. 57, 853–865.

Grégoire, S., Cubberley, R., Duplan, H., Eilstein, J., Lange, D., Hewitt, N., Jacques-Jamin, C., Klaric, M., Rothe, H., Ellison, C., Vaillant, O., Schepky, A., 2017. Solvent solubility testing of cosmetics-relevant chemicals: methodology and correlation of water solubility to in silico predictions. J. Soln. Chem. 46 (7), 1349–1363.

Gregoire, S., Cubberley, R., Duplan, H., Eilstein, J., Hewitt, N., Jacques-Jamin, C., Genies, C., Klaric, M., Rothe, H., Ellison, C., Fernandez, J., Schepky, A., 2019. Use of a simple in vitro test to assess loss of chemical due to volatility during an in vitro human skin absorption study. Skin Pharmacol. Physiol. 32 (3), 117–124.

Gregoire, S., Sorrell, I., Lange, D., Najjar, A., Schepky, A., Ellison, C., Troutman, J., Fabian, E., Duplan, H., Genies, C., Jacques-Jamin, C., Klaric, M., Hewitt, N.J., 2021. Cosmetics Europe evaluation of 6 in silico skin penetration models. Computat. Toxicol. 19, 100177.

Hamadeh, A., Troutman, J., Edginton, A.J., 2021. Assessment of vehicle volatility and deposition layer thickness in skin penetration models. Pharmaceutics 13, 807.

Hansen, S., Selzer, D., Schaefer, U.F., Kasting, G.B., 2011. An extended database of keratin binding. J. Pharm. Sci. 100 (5), 1712–1726.

Hanson, K.M., Behne, M.J., Barry, N.P., Mauro, T.M., Gratton, E., Clegg, R.M., 2002. Two-photon fluorescence lifetime imaging of the skin stratum corneum pH gradient. Biophys. J. 83 (3), 1682–1690.

Hayduk, W., Laudie, H., 1974. Prediction of diffusion coefficients for nonelectrolytes in dilute aqueous solutions. Am. Inst. Chem. Eng. J. 20 (3), 611–615.

Hewitt, N.J., Grégoire, S., Cubberley, R., Duplan, H., Eilstein, J., Ellison, C., Lester, C., Fabian, E., Fernandez, J., Géniès, C., Jacques-Jamin, C., Klaric, M., Rothe, H., Sorrell, I., Lange, D., Schepky, A., 2019. Measurement of the penetration of 56 cosmetic relevant chemicals into and through human skin using a standardized protocol. J. Appl. Toxicol. 40 (3), 403–415.

Hoffmann, S., Alépée, N., Gilmour, N., Kern, P.S., van Vliet, E., Boislève, F., Bury, D., Cloudet, E., Klaric, M., Kühnl, J., Lalko, J.F., Mewes, K., Miyazawa, M., Nishida, H., Tam Brami, M.T., Varçin, M., Api, A.M., Europe, C., 2022. Expansion of the Cosmetics Europe skin sensitisation database with new substances and PPRA data. Regul. Toxicol. Pharm. 131, 105169.

Ibrahim, R., Nitsche, J.M., Kasting, G.B., 2012. Dermal clearance model for epidermal bioavailability calculations. J. Pharm. Sci. 101 (6), 2094–2108.

Intarakumhaeng, R., Li, S.K., 2014. Effects of solvent on percutaneous absorption of non-volatile lipophilic solute. Int. J. Pharm. 476 (1–2), 266–276.

Intarakumhaeng, R., Wanasathop, A., Li, S.K., 2018. Effects of solvents on skin absorption of non-volatile lipophilic and polar solutes under finite dose conditions. Int. J. Pharm. 536 (1), 405–413.

Jaworska, J.S., Natsch, A., Ryan, C., Strickland, J., Ashikaga, T., Miyazawa, M., 2015. Bayesian integrated testing strategy (ITS) for skin sensitization potency assessment: a decision support system for quantitative weight of evidence and adaptive testing strategy. Arch. Toxicol. 89 (12), 2355–2383.

Kasting, G.B., Miller, M.A., 2006. Kinetics of finite dose absorption through skin 2. Volatile compounds. J. Pharm. Sci. 95 (2), 268–280.

Kasting, G.B., Miller, M.A., LaCount, T.D., Jaworska, J., 2019. A composite model for the transport of hydrophilic and lipophilic compounds across the skin. J. Pharm. Sci. 108, 337–349.

Kasting, G.B., Miller, M.A., Xu, L., Yu, F., Jaworska, J., 2022. In vitro human skin absorption of solvent-deposited solids: niacinamide and methyl nicotinate. J. Pharm. Sci. 111 (3), 727–733.

Kretsos, K., Miller, M.A., Zamora-Estrada, G., Kasting, G.B., 2008. Partitioning, diffusivity and clearance of skin permeants in mammalian dermis. Int. J. Pharm. 346 (1-2), 64–79.

Levin, J., Maibach, H., 2008. Human skin buffering capacity: an overview. Skin Res. Technol. 14 (2), 121–126.

Li, X., Johnson, R., Weinstein, B., Wilder, E., Smith, E., Kasting, G.B., 2015. Dynamics of water transport and swelling in human stratum corneum. Chem. Eng. Sci. 138, 164–172.

Li, X., Johnson, R., Kasting, G.B., 2016. On the variation of water diffusion coefficient in stratum corneum with water content. J. Pharm. Sci. 105 (3), 1141–1147.

Miller, M.A., Kasting, G.B., 2015. A spreadsheet-based method for simultaneously estimating the disposition of multiple ingredients applied to skin. J. Pharm. Sci. 104 (6), 2047–2055.

Miller, M.A., Kasting, G.B., 2022. Absorption of solvent-deposited weak electrolytes and their salts through human skin in vitro. Int. J. Pharm. 620, 121753.

Morrison, G.C., Weschler, C.J., Beko, G., 2016. Dermal uptake directly from air under transient conditions: advances in modeling and comparisons with experimental results for human subjects. Indoor Air 2016, 12277.

Natsch, A., Haupt, T., Wareing, B., Landsiedel, R., Kolle, S., 2020. Predictivity of the kinetic direct peptide reactivity assay (kDPRA) for sensitizer potency assessment and GHS subclassification. ALTEX 37, 652–664.

Nitsche, J.M., Frederick Frasch, H., 2011. Dynamics of diffusion with reversible binding in microscopically heterogeneous membranes: general theory and applications to dermal penetration. Chem. Eng. Sci. 66 (10), 2019–2041.

Nitsche, J.M., Kasting, G.B., 2022. A framework for incorporating transient solute-keratin binding Into dermal absorption models. J. Pharm. Sci. 111 (7), 2093–2106.

Nitsche, J.M., Wang, T.-F., Kasting, G.B., 2006. A two-phase analysis of solute partitioning into the stratum corneum. J. Pharm. Sci. 95 (3), 649–666.

Poling, B.E., Prausnitz, J.M., O'Connell, J.P., 2001. The Properties of Gases and Liquids, 5th ed. McGraw-Hill, New York.

Roberts, D.W., Aptula, A.O., Patlewicz, G., Pease, C., 2008. Chemical reactivity indices and mechanism-based read-across for non-animal based assessment of skin sensitisation potential. J. Appl. Toxicol. 28 (4), 443–454.

Roberts, D.W., Natsch, A., 2009. High throughput kinetic profiling approach for covalent binding to peptides: application to skin sensitization potency of Michael acceptor electrophiles. Chem. Res. Toxicol. 22 (3), 592–603.

Ryan, C.A., Troutman, J.A., Kern, P.S., Quijano, M., Dobson, R.L.M., Dai, H.J., Burt, T.M., Gerberick, G.F., 2020. Refinement of the peroxidase peptide reactivity assay and prediction model for assessing skin sensitization potential. Tox. Sci. 178, 88–103.

Saadatmand, M., Stone, K.J., Vega, V.N., Felter, S., Ventura, S., Kasting, G., Jaworska, J., 2017. Skin hydration analysis by experiment and computer simulations and its implications for diapered skin. Skin Pharmacol. Physiol. 23 (4), 500–513.

Scheuplein, R.J., 1978. Skin permeation. In: Jarrett, A. (Ed.), The Physiology and Pathophysiology of the Skin. Academic Press, New York, pp. 1669–1752.

Scheuplein, R.J., Ross, L.W., 1974. Mechanism of percutaneous absorption V. Percutaneous absorption of solvent deposited solids. J. Invest. Dermatol. 62 (4), 353–360.

Schwobel, J.A.H., Koleva, Y.K., Enoch, S.J., Bajot, F., Hewitt, M., Madden, J.C., Roberts, D.W., Schultz, T.W., Cronin, M.T.D., 2011. Measurement and estimation of electrophilic reactivity for predictive toxicology. Chem. Rev. 111 (4), 2562–2596.

Schwobel, J.A.H., Ebert, A., Bittermann, K., Huniar, U., Goss, K.-U., Klamt, A., 2020. COSMOperm: mechanistic prediction of passive membrane permeability for neutral compounds and ions and its pH dependence. J. Phys. Chem. B 124 (16), 3343–3354.

Seif, S., Hansen, S., 2012. Measuring the stratum corneum reservoir: desorption kinetics from keratin. J. Pharm. Sci. 101 (10), 3718–3728.
US_EPA, 2011. Estimation Programs Interface SuiteTM for Microsoft® Windows Vers 4.1. U.S. Environmental Protection Agency, Washington, DC, USA.
Vickers, C.F., 1963. Existence of reservoir in stratum corneum. Experimental proof. Arch. Dermatol. 88, 21–23.
Vickers, C.F., 1972. Stratum corneum reservoir for drugs. Adv. Biol. Skin 12, 177–189.
Wang, T.-F., Kasting, G.B., Nitsche, J.M., 2006. A multiphase microscopic model for stratum corneum permeability. I. Formulation, solution and illustrative results for representative compounds. J. Pharm. Sci. 95, 620–648.
Wang, T.-F., Kasting, G.B., Nitsche, J.M., 2007. A multiphase microscopic model for stratum corneum permeability. II. Estimation of physicochemical parameters and application to a large permeability database. J. Pharm. Sci. 96, 3024–3051.
Wareing, B., Kolle, S., Natsch, A., Haupt, T., 2020a. Kinetic Direct Peptide Reactivity Assay (kDPRA): validation study report. OECD, Paris, France.
Wareing, B., Kolle, S.N., Birk, B., Alépée, N., Haupt, T., Kathawala, R., Kern, P.S., Nardelli, L., Raabe, H., Rucki, M., Ryan, C.A., Verkaart, S., Westerink, W.M.A., Landsiedel, R., Natsch, A., 2020b. The kinetic Direct Peptide Reactivity Assay (kDPRA): intra- and inter-laboratory reproducibility in a seven-laboratory ring trial. ALTEX 37, 639–651.
Wilke, C.R., Chang, P., 1955. Correlation of diffusion coefficients in dilute solutions. AIChE J 1 (2), 264–270.
Williams, F.M., Rothe, H., Barrett, G., Chiodini, A., Whyte, J., Cronin, M.T.D., Monteiro-Riviere, N.A., Plautz, J., Roper, C., Westerhout, J., Yang, C., Guy, R.H., 2016. Assessing the safety of cosmetic chemicals: Consideration of a flux decision tree to predict dermally delivered systemic dose for comparison with oral TTC (Threshold of Toxicological Concern). Reg. Toxicol. Pharmacol. 76, 174–186.
Yadav, S., Pinto, N.G., Kasting, G.B., 2007. Thermodynamics of water interaction with human stratum corneum. I. Measurement by isothermal flow calorimetry. J. Pharm. Sci. 96, 1585–1597.
Yu, F., Tonnis, K., Kasting, G.B., Jaworska, J., 2021. Computer simulation of skin permeability of hydrophobic and hydrophilic chemicals: Influence of follicular pathway. J. Pharm. Sci. 110 (5), 2149–2156.
Yu, F., Tonnis, K., Xu, L., Jaworska, J., Kasting, G.B., 2022. Modeling the percutaneous absorption of solvent-deposited solids over a wide dose range. J. Pharm. Sci. 111 (3), 769–779.